Massachusetts Bay Eutrophication Model: 2005 Simulation

Massachusetts Water Resources Authority
Environmental Quality Department
Report 2008-13

Jiang MS, Zhou M. 2008. **Massachusetts Bay Eutrophication Model: 2005 Simulation**. Boston: Massachusetts Water Resources Authority. Report 2008-13. 82 pp.

Massachusetts Water Resources Authority
Boston, Massachusetts

Massachusetts Bay Eutrophication Model: 2005 Simulation

Prepared by:
Mingshun Jiang & Meng Zhou
Department of Environmental, Earth and Ocean Sciences
University of Massachusetts Boston
100 Morrissey Blvd
Boston, MA 02125

July 2008

EXECUTIVE SUMMARY

Under an agreement between the University of Massachusetts Boston (UMB) and Massachusetts Water Resources Authority (MWRA), the UMB modeling team has been maintaining, enhancing and applying the existing hydrodynamic and water quality models for the Boston Harbor, Massachusetts Bay and Cape Cod Bay system (MBS). Five years (2000-2005) of simulations have been conducted since 2001. This report presents the validation of the Massachusetts Bay (MB) water quality model (also called Bays Eutrophication Model, BEM) for 2005 and an impact analysis of MWRA effluent nutrients on algal blooms in the MBS.

This study concludes that the modeled water quality variables are comparable to the observed ones in the period 2005 with relative improvements compared to the 1998-2004 simulations. The model results represent the physical, biological and chemical environment and processes in the water column and sediments in the MBS:

1. Seasonal cycles:
   - Surface nutrient enrichment due to vertical mixing
   - Nutrient depletion due to phytoplankton intake and onset of stratification
   - Spring and fall diatom-dominated blooms
   - Flagellate blooms due to onset of silica depletion
   - Fluctuations of nutrient regeneration and dissolved oxygen (DO) during the summer
   - Seasonal changes in transport–retention of biota associated with seasonal circulation patterns
2. Short term responses:
   - Upwelling and downwelling winds
   - Mesoscale eddies along the coast and CCB (Cape Cod Bay)
   - Episodic phytoplankton bloom events

The model has similar difficulties as in previous simulations in simulating chlorophyll and bottom PON concentrations in general and primary production in summer. The causes for these mismatches between model and observed results are made complex by the natural complexity of the ecosystem, uncertainties in empirical formulas of many processes, and the limitation of model schemes and resolutions. All of these need to be further investigated.

The impact analysis of MWRA effluent nutrients suggests a strong seasonal cycle in spatial pattern and magnitude. In spring, when the coastal current is southward corresponding to the GOM (Gulf of Maine) current intrusion and northerly or northeasterly winds, the effluent is quickly transported southward along the western coast. In summer and fall, the effluent is trapped below the thermocline but intermittent upwelling events caused by southwesterly winds may bring these waters into the surface layer. Average over western MB (an area extending to the Stellwagen Basin in the east and the northern boundary of Cape Cod Bay in the south), the effluent may lead to a 10-20% increase in local DIN (dissolved inorganic nitrogen) concentrations during spring

and less than 10% in the remainder of the year. The effluent may enhance local chlorophyll concentrations less than 10%. These results are consistent with earlier simulation results and data analysis.

A nutrient budget analysis for May 2005 suggests that the primary production was nutrient–limited prior to the first Nor'easter wind storm, and the vertical mixing in two Nor'easter wind storms contributed a large amount of nutrients (60% of total nutrients) to the surface mixed layer which supported a high primary production rate of 1.5 $gC/m^2/day$ for 30 days. Rivers and background vertical mixing supplied about 15% of the nutrients required by primary production. MWRA and atmospheric loading contributed less than 2% each.

This analysis also suggests that in late spring, primary productivity in the MBS is normally nutrient–limited.

These new findings and understanding have indicated areas for further improvement:

1) Better understanding and estimates of the intruding GOM coastal current off Cape Ann, which primarily determines the general circulation strength, patterns and salinity in the MBS;
2) Better understanding of mesoscale physical-biogeochemical processes such as eddy formation and translation in northern Mass Bay associated with northeasterly wind events, and the transport and dispersion of effluent associated with these eddies;
3) Better understanding of *Phaeocystis* and red tide blooms associated with physical processes and nutrient dynamics in the MBS, and development of models to simulate the physiology and behavior of these algal species; and
4) Optimizing the spatial and temporal coverage of observations at open boundaries and in the interior for improving model quality.

TABLE OF CONTENTS

LIST OF FIGURES

LIST OF TABLES

1. INTRODUCTION

1.1 Project overview

This report is Part II of the report on the 2005 hydrodynamic and water quality simulation for the Boston Harbor (BH), Massachusetts Bay (MB) and Cape Cod Bay (CCB) system (all of which constitute the Massachusetts Bays System (MBS)) supported by the Massachusetts Water Resources Authority (MWRA) under subcontract to their contract with Battelle. This report presents the water quality results from the Bays Eutrophication Model (BEM). Details on projects and histories can be found in Part I: The Massachusetts and Cape Cod Bays Hydrodynamic Model: 2005 Simulation (Jiang and Zhou 2008).

1.2 Physical setting

Studies have indicated that the circulation in the MBS varies in response to 1) wind stresses and heat fluxes at the sea surface, 2) tides and mean surface slopes at the open boundary, and 3) freshwater runoff including outfall effluent (Geyer et al., 1992; Signell et al., 1996; Jiang and Zhou, 2004a; Jiang and Zhou, 2006a). The yearly mean current in the MBS is characterized by a counterclockwise circulation, which is primarily driven by the western GOM coastal current intruding through the North Passage, local freshwater runoff, and surface heating. The water column stratification varies seasonally. Stratification occurs in spring due to both freshwater runoff and surface heating, and is intensified and reaches a maximum strength during summer. The water column stratification breaks down in the fall due to surface cooling and increasing wind mixing, and the water column is well mixed in winter.

As early as 1927, Bigelow suggested that the WMCC (Western Maine Coastal Current) breaks into two branches at Cape Ann: one intrudes deeply into the MBS, and another follows the outer edge of the Stellwagen Bank (Bigelow, 1927; Lynch et al., 1996). This bifurcation is determined by the nonlinear interactions between topography, coastlines, freshwater plume from the Merrimack River, and the WMCC. The volume transport of this intruding current primarily determines the circulation in the MBS. It circulates counterclockwise along western Massachusetts Bay and frequently penetrates

into CCB, especially in winter and spring seasons (Geyer et al., 1992; Jiang and Zhou, 2004a).

Previous studies indicated pronounced seasonal variations in the circulation pattern (Geyer et al., 1992; HydroQual and Signell, 2001; Signell et al., 1996; Butman, et al., 2002; Jiang and Zhou, 2004a). In western MB, surface currents are strongly driven by winds. In winter and spring seasons, northerly winds drive a southward coastal current creating a counterclockwise circulation. In summer and early fall, predominantly southwesterly winds produce offshore Ekman transport and coastal upwelling, which induce a northward coastal current along the upwelling front at the western coast.

1.3 Biological environment

Phytoplankton growth in the MBS is primarily driven by nutrients, temperature and photosynthetically available radiation (PAR) (Libby et al., 2000; Libby et al., 2001). The spring bloom is triggered by the onset of stratification and strengthened with the increase in solar radiation. The available nitrogen and silica in a well-mixed water column during winter lead to the dominance of diatoms. In late spring and summer, stratification suppresses vertical mixing at thermocline and limits upward nutrient fluxes, which in turn limits the primary production in the MBS. The abundance of phytoplankton cells usually reaches a maximum at mid-summer with exceptions. The late summer assemblage is comprised primarily of dinoflagellates and mixed species of diatoms, mainly the genus *Chaetoceros*. The fall bloom typically occurs in late September when strong mixing produced by wind and surface cooling breaks down water column stratification and brings nutrients from deep water to the euphotic zone. The primary production declines in November as solar radiation decreases and mixing further increases.

Abundant phytoplankton in the MBS supports abundant zooplankton, ranging from 10 to 50×10^3 individuals m^{-3} (Turner, 1994; Libby et al., 2001; Libby et al., 2002). In winter, zooplankton assemblages are dominated by copepod nauplii, *Oithona similis* females and copepodites, gastropod veligers, and *Acartia hudsonica* females and copepodites. In late winter and early spring, in addition to these dominant species, subdominant species are bivalve veligers, copepodites of *Calanus finmarchicus*, *Pseudocalanus* and *Temora longicornis*, and *Oikopleura dioica*. In summer and early fall,

marine cladoceran *Evadne nordmanni*, *Microsetella norvegica* and copepodites of the genus *Centropages* are added to the species spectrum. Zooplankton transfer the biomass from primary producers to higher trophic levels such as fish and mammals.

The sea floor in the MBS is complicated, with a variety of bottom types. Soft-bottom occupies most areas in BH, CCB and Stellwagen Basin, while hard-bottom dominates the shallow nearshore areas. The annelid worms are most abundant in soft-bottom communities, accounting for more than 80% of the fauna at most MWRA monitoring stations, and crustaceans are second most abundant fauna (Kropp et al., 2001; Kropp et al., 2002; Maciolek et al., 2003). The dominant taxa in hard-bottom communities are algae, including *Lithothamnion spp*., dulse, and red filamentous species. The dominant animal taxa include *Asterias vulgaris* and the horse mussel *Modiolus modiolus*.

The benthic processes in BH are dominated by local biological processes, while in MB and CCB they are generally influenced by region-wide physical and biological processes (Tucker et al., 2006). High sediment oxygen demand (SOD) and fluxes of dissolved inorganic nitrogen have been observed in the harbor, both of which have been decreasing in the last decade due to the reduction in pollutant loadings to the harbor. Intensive denitrification also occurs in the harbor, and its relative role in the nitrogen budget has increased since the outfall relocation. Sediments in the MBS are well oxygenated; and denitrification accounts for about half of the total DIN flux. No obvious seasonal pattern in DIN fluxes has been observed. On the contrary, the SOD fluxes exhibit strong seasonal patterns, which are well correlated with the bottom temperature.

Most of these processes are simulated in the BEM, which focuses on the nutrient cycling and related oxygen processes, including phytoplankton growth (primary production), transformation of phytoplankton biomass into various forms of organic matter, and regeneration of inorganic nutrients occurring in both the water column and sediments. The physical processes are simulated by the hydrodynamic model (Jiang and Zhou 2008). The bulk of phytoplankton species are represented as three functional groups representing the species composition during winter/spring, summer, and fall, respectively. Activities of both zooplankton and the benthic community are simply parameterized. The model structure of the BEM and model implementation will be described in Section 2.

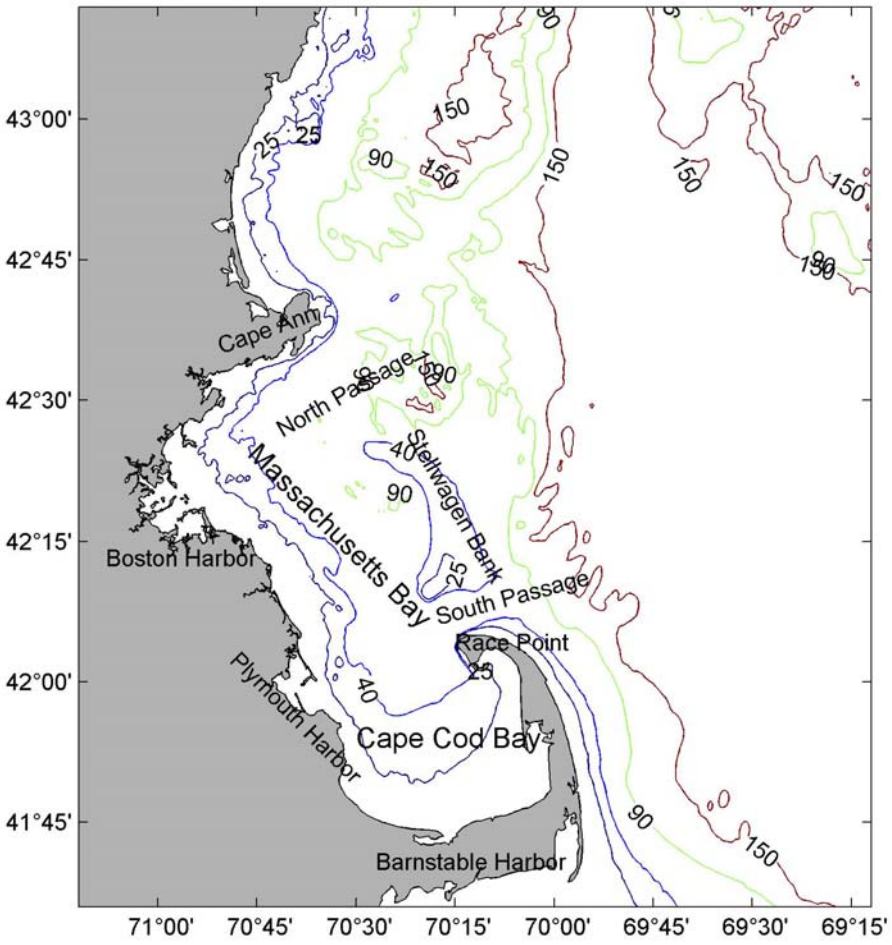

Figure 1.1. Bathymetry in the Boston Harbor, Massachusetts Bay and Cape Cod Bay system.

2. MODEL DESCRIPTION

2.1 Model domain and grid

The BEM grid is essentially the same as the grid used for the hydrodynamic model with two modifications: 1) the model domain covers the entire MBS with the open boundary starting from Cape Ann to the outer edge of Cape Cod (Figure 2.1), that is, those grid cells east of this boundary in the hydrodynamic model are eliminated in the BEM; and 2) the top 3 sigma layers in the hydrodynamic model are integrated to 1 sigma layer in the BEM. Therefore, the BEM has 54×68 horizontal grid cells and 10 vertical layers.

2.2 Nutrient dynamics

The water quality model describes the phytoplankton growth and nutrient cycling through a number of prognostic variables and a set of differential equations, which govern the temporal and spatial changes of these variables based on fluid motion, biogeochemical process rates and mass conservation. Key biological and chemical processes included in these equations are based on theoretical and empirical relationships and parameters. The current BEM has 26 prognostic variables, which include salinity, three phytoplankton groups, four types of nutrients (C, N, P, Si) and related organic components, dissolved oxygen, aqueous oxygen, and trace metals, and more than 100 model parameters (Tables 2.1 and 2.2). The three phytoplankton groups represent winter/spring, summer, and fall algal assemblages, respectively, with different carbon-to-chlorophyll ratios, uptake ratios of nutrients, and other physiological properties. The BEM also has a sediment sub-model to simulate the biogeochemical processes in the sediment and fluxes between the water column and sediment.

The model structure for the nitrogen cycle is shown in Figure 2.2. The central process is phytoplankton photosynthesis, which transforms dissolved inorganic nitrogen (DIN) to phytoplankton biomass. DIN includes ammonium (NH_4), nitrate (NO_3) and nitrite (NO_2). For the modeling, the latter two are combined and denoted as NO_3. NH_4

can be transformed into NO_3 through nitrification. The living cells of phytoplankton can be transformed into non-living organic matter by respiration, mortality and zooplankton grazing. The zooplankton grazing is accounted for as instantaneous removal of phytoplankton standing stocks, which is subject to temperature modulation with a maximum of 10%. There are two non-living organic nitrogen types, dissolved organic nitrogen (DON) and particulate organic nitrogen (PON). They are further divided into refractory (RDON and RPON) and labile (LDON and LPON) forms. LDON and LPON are decomposed much faster than RDON and RPON. However, PON in section 3 will also include living cells (phytoplankton). The regeneration process of organic matter involves two steps: 1) particles break down to DON, and 2) DON is further remineralized to ammonia. Particles settled down into sediments will be decomposed and feed back to the water column through fluxes of NO_3 and NH_4. The sediment denitrification will produce N_2 gas, which is simply lost from the system. In addition to these internal cycling processes, the water column receives inputs of nitrogen from land sources as runoff and effluent containing inorganic and organic nutrients, from the atmosphere through gas exchange, and from open boundaries (see Section 2.3.2 and 2.3.3). Mathematical equations for these processes can be found in HydroQual and Normandeau (1995). For the convenience of the reader, they are also included in Appendix A.

The cycling processes of carbon and phosphorus have similar structures to that of nitrogen. However, each of them has only one dissolved inorganic form and dissolved organic carbon has two additional forms (see Table 2.1). The oxygen cycling generally follows the cycling of carbon in the water column, while the exchange of oxygen with the air is driven by wind entrainment and solubility at the surface. Silicon has only one dissolved inorganic form (SiO_4) and one biogenic form (BSi). Detailed descriptions can be found in earlier reports of this model (HydroQual, 2000; HydroQual, 2003; HydroQual and Normandeau, 1995; Jiang and Zhou, 2004b).

The sediment biogeochemical processes in the BEM are governed by a sediment sub-model (Di Toro, 2001). Particulate organic matter in the water column settles down into the sediment, and is remineralized by sediment diagenesis. Fluxes of dissolved nutrients and sediment oxygen demand (SOD) through the water-sediment interface represent the interactions between biogeochemical processes in the water column and sediment.

Nitrogen gas released by the denitrification process is removed from the system through outgassing to the atmosphere. Re-suspension of sediments is simulated in the BEM by recycling 40% of the sinking fluxes back into the water column.

2.3 Forcing

2.3.1 Surface forcing

The surface forcing in the BEM includes solar radiation (provided by WHOI), day length and wind (measured at NOAA 44013) (Figure 2.3). The winter experiences shortest daylight and lowest solar radiation while the summer has the longest daylight and strongest radiation. Winds also exhibit a strong seasonal pattern with the strongest winds in winter and weakest in summer (Jiang and Zhou, 2008). Two strong Nor'easters occurred in May 2005, which can be clearly seen from the wind speed data. Wind forcing determines the air-sea gas exchange, which is formulated as Hyer et al. (1971), and affects the biogeochemical processes indirectly through vertical mixing and horizontal transport. Solar radiation and day length determine the photosynthesis of phytoplankton. To account for the photo-adaptation of phytoplankton, the average solar radiation in the previous three days is used as the current saturation solar radiation (see Appendix A).

2.3.2 Nutrient loadings

In addition to loadings from the GOM through the open boundary, the MBS receives large nutrient (including inorganic and organic matter) inputs from point sources including sewage effluents and river discharges. Other nutrient sources in the MBS include nonpoint sources (NPS) (CSO, stormwater, and groundwater) and atmospheric inputs. The daily mean nutrient loadings of MWRA effluent and river discharges were calculated and updated every year based on observed nutrient concentrations and flow rates except that the multiple–yearly averaged carbon concentrations in river discharges were used. The nonpoint source loadings were calculated by HydroQual (HydroQual, 2003) based on the estimates of Menzie-Cura and Associates (1991). The non-MWRA

effluent loadings used the same values as in the 2000-2001 simulation, which was partially updated by using the latest CSO data provided by the MWRA (Jiang and Zhou, 2004b). The atmospheric loadings were the same as in previous simulations (HydroQual, 2003; Jiang and Zhou, 2004b).

Within these inputs, the MWRA effluent is the dominant source for nitrogen and phosphorus (Figure 2.4). Among the other sources, non-MWRA wastewater treatment plant (WWTP) effluent is the largest for phosphorus and the atmosphere provides most of the remaining nitrogen. Though the phosphorus loading in the MWRA effluent decreased in 2005, the carbon loading increased slightly in 2005. The total nitrogen loading in recent years has remained nearly unchanged compared to that of the period from 1992 to 2004 (see, e.g., HydroQual, 2003, Jiang and Zhou, 2004b, 2006b). We note that previous modeling and observational estimates indicate that the MWRA nutrient loadings are only 3~6% of the nutrient loadings from the GOM (Adams et al., 1992; Becker, 1992; HydroQual, 2000).

The total loading is converted to loadings of different components because only the total loading of an individual organic component is available for MWRA effluent and other sources. For example, the total organic nitrogen loading is separated into LPON, RPON, LDON and RDON. The partition coefficients for each nutrient in the previous simulations (1998-1999, 2000-2004) were used in the 2005 model run (Table 2.3) (HydroQual, 2000; HydroQual, 2003; HydroQual and Normandeau, 1995; Jiang and Zhou, 2004b; Jiang and Zhou, 2006b).

2.3.3 Open boundary conditions

The open boundary conditions for the 2005 simulation were constructed based on the same objective interpolation procedures and software (OAX) used for the construction of open boundary conditions for the hydrodynamic model (Hendry and He, 1996). Because there are insufficient data to compute the spatial and temporal de-correlation scales, the correlation function was specified as follows,

$$R(r) = \left(1 + r + \frac{r^3}{3}\right)\exp(-r) \tag{2.1}$$

where r is the pseudo-distance between the data point and the target point,

$$r = \sqrt{\left(\frac{x - x_0}{a}\right)^2 + \left(\frac{y - y_0}{a}\right)^2 + \left(\frac{z - z_0}{b}\right)^2 + \left(\frac{t - t_0}{T}\right)^2} \tag{2.2}$$

where a, b, and T are the horizontal, vertical and temporal correlation scales, respectively. Because the OAX is based on the statistics, the relative error is estimated during interpolation as the root–mean–squares (rms). The data used for constructing the open boundary for 2005 were collected by the MWRA monitoring program, MWRA *Alexandrium* Rapid Response Surveys, and Stellwagen Bank National Marine Sanctuary (Figure 2.5). The data collected by Harbor Monitoring Program (e.g. Taylor, 2004) were not used in constructing the boundary conditions because these stations were too far away from the open boundary. The horizontal, vertical and temporal correlation scales were 20 km, 15m and 15 day, respectively, which were chosen to ensure that the results rely mainly on the observations near the open boundary. During the months when there were no data collected at those stations near the open boundary (F26, F27, F28 and F29), the interpolation had to select data collected along the boundary in neighboring months or had to rely on data at other stations for the same month but inside the MBS. Obviously significant uncertainties would be introduced. Since a model prediction was determined by a combination of biogeochemical processes, local forcing, and open boundary conditions, a less accurate open boundary condition would lead to a less accurate prediction. The overall quality of data coverage is shown in Table 2.4. The quality of boundary conditions was dependent on the available observations along the boundary in some months.

The interpolated organic matter values were further separated into labile and refractory forms based on the partition coefficients used in previous simulations (Table 2.3). Data for phytoplankton biomass were insufficient to construct the open boundary conditions directly because the measurements were only taken at a few monitoring stations. As an alternative, chlorophyll data were used and converted to phytoplankton biomass. A total chlorophyll value was divided based on empirical percentages of 3 individual groups (Table 2.5) and then the chlorophyll value for each group was converted to the biomass using the ratio of carbon to chlorophyll (CChl). These group

partitions and ratios of carbon to chlorophyll were the same as to those used in previous BEM simulations (Jiang and Zhou, 2004b, 2006b).

Most variables at the open boundary showed significant vertical and horizontal variations in April (Figure 2.6). For example, the subsurface chlorophyll maximum was present along the open boundary, and both nitrate and ammonia concentrations were low within the mixed layer. Nutrient concentrations decreased from the north to the south, which suggests that the MBS was importing nutrients from the GOM in the North Passage. Higher organic matter concentrations were found in the North Passage than in the South Passage which is different from the distribution in a normal year when the local production in the MBS contributes higher organic matter concentrations in the South Passage than those of the North Passage. These abnormal organic matter concentration gradients were likely produced by the earlier peaks of river flows in 2005 (Jiang and Zhou, 2008). Oxygen concentration showed a strong vertical gradient and a weak horizontal gradient with the maximum concentration located in the north boundary.

The surface nutrients were nearly depleted in August, and the horizontal nutrient gradients were much less than those in April (Figure 2.7). A weak subsurface maximum and a weak horizontal gradient of DO were found. However, the horizontal and vertical gradients of organic matter were similar to those in April.

These procedures using the objective interpolation methods to construct open boundary conditions preserved the spatial and temporal features of observations while providing an estimate of statistical errors. Compared to the boundary conditions constructed manually with unknown errors (HydroQual, 2003), the objective interpolation tracks the details of how the boundary conditions are constructed and their potential errors.

2.4 Numerical scheme

The BEM is offline-coupled with the hydrodynamic model, which is ECOM-si (HydroQual, 2000). The modeled hydrodynamic variables such as temperature, salinity, currents and turbulent mixing coefficients from the hydrodynamic model were averaged

every hour and stored. These data were input into the water quality model as the physical forcing. In the BEM, the top 3 layers in ECOM-si were integrated into one top layer in the same way as during previous runs. A collapse program was used to average hydrodynamic variables in the top 3 layers of ECOM-si and assigned the resulting values to the top sigma layer in the BEM. The time dependent advection-diffusion-reaction equations in the BEM were integrated using the explicit upwind scheme and the Smolarkiewicz flux-correction algorithm (Smolarkiewicz, 1984). The variables at the open boundary were specified using the values derived from the objective interpolation and partitioning as discussed above.

2.5 Model parameters

All model parameters used in the 2005 simulation were the same as those in the 1998-99 and 2000-2004 simulations (HydroQual, 2003, Jiang and Zhou, 2004b; Jiang and Zhou, 2006b). The value of light attenuation is spatially variable ranging from 0.6 m^{-1} in Boston Harbor to 0.16 m^{-1} offshore, which was calculated based on the light transmissivity data collected during the outfall monitoring program (HydroQual and Signell, 2001). These parameters and their values are shown in tables 2.1-2.2.

2.6 Initial conditions

The initial conditions for 2005 were derived from modeled results at the end of 2004, i.e. no spin-up was used in the simulation.

2.7 Aggregation and filtering

Various aggregation and filtering have been used for the forcing data, and for model output and validation data (section 3); these are listed in Table 2.6.

Table 2.1 Model variables[1]

No.	Variables	Units
1	Salinity	ppt
2	Phytoplankton winter/spring group (diatoms)	mg C l^{-1}
3	Phytoplankton summer group	mg C l^{-1}
4	Phytoplankton fall group	mg C l^{-1}
5	Particulate organic phosphorous – refractory component	mg P l^{-1}
6	Particulate organic phosphorous – labile component	mg P l^{-1}
7	Dissolved organic phosphorous – refractory component	mg P l^{-1}
8	Dissolved organic phosphorous – labile component	mg P l^{-1}
9	Total dissolved inorganic phosphorous	mg P l^{-1}
10	Particulate organic nitrogen – refractory component	mg N l^{-1}
11	Particulate organic nitrogen – labile component	mg N l^{-1}
12	Dissolved organic nitrogen – refractory component	mg N l^{-1}
13	Dissolved organic nitrogen – labile component	mg N l^{-1}
14	Total ammonia (ammonia in water and phytoplankton cell)	mg N l^{-1}
15	Nitrite + nitrate	mg N l^{-1}
16	Biogenic silica	mg Si l^{-1}
17	Total silica – (silica in water and phytoplankton cell)	mg Si l^{-1}
18	Particulate organic carbon – refractory component	mg C l^{-1}
19	Particulate organic carbon – labile component	mg C l^{-1}
20	Dissolved organic carbon – refractory component	mg C l^{-1}
21	Dissolved organic carbon – labile component	mg C l^{-1}
22	Dissolved organic carbon – reactive component	mg C l^{-1}
23	Dissolved organic carbon – algal exudate	mg C l^{-1}
24	O_2* - aqueous oxygen	mg O_2 l^{-1}
25	Dissolved oxygen	mg O_2 l^{-1}
26	Total active metal (TAM)	mmol l^{-1}

[1] The relationships between these model parameters and some of the output variables such as DIN, DON and PON, are discussed in the main text.

Table 2.2. Model parameters for nitrogen cycle

Notation	Description	Values
Diatoms (winter/spring group) growth, carbon to nitrogen ratios and carbon to chlorophyll ratios		
T_{opt1}	Optimal growth temperature	8 ºC
β_{11}	Temperature correction coefficient on growth rate	0.004 (ºC)$^{-2}$
β_{21}	Temperature correction coefficient on growth rate	0.006 (ºC)$^{-2}$
G_{pre1}	Gross photosynthetic rate	2.5 day^{-1}
G_{pr01}	Nutrient-saturated gross photosynthetic rate per unit light intensity	0.28 m^2(mol quanta)$^{-1}$
k_{N1}	Half saturation constant for nitrogen uptake	0.01 mg N l^{-1}
k_{RB1}	Basal respiration rate	0.03 day^{-1}
k_{RG1}	Growth-rate-dependent respiration coefficient	0.28
k_{grz01}	Mortality rate due to grazing	0.1 day^{-1}
θ_{grz1}	Temperature dependent coefficient for grazing	1.1
f_{sc1}	Fraction of C allocated to structural purposes	0.1
W_{CChl1}	Nutrient-saturated carbon to chlorophyll ratio	40 mgC (mgChl a)$^{-1}$
QF_1	Quotient of nutrient-limited N:C ratio	0.85
W_{CN1}	Nutrient-saturated carbon to nitrogen ratio	5.0 mgC (mgN)$^{-1}$
Summer group growth, carbon to nitrogen ratios and carbon to chlorophyll ratios		
T_{opt2}	Optimal growth temperature	18 ºC
β_{12}	Temperature correction coefficient on growth rate	0.004 (ºC)$^{-2}$
β_{22}	Temperature correction coefficient on growth rate	0.006 (ºC)$^{-2}$
G_{pre2}	Gross photosynthetic rate	3.0 day^{-1}
G_{pr02}	Nutrient-saturated gross photosynthetic rate per unit light intensity	0.28 m^2(mol quanta)$^{-1}$
k_{N2}	Half saturation constant for nitrogen uptake	0.01 mg N l^{-1}
k_{RB2}	Basal respiration rate	0.036 day^{-1}
k_{RG2}	Growth-rate-dependent respiration coefficient	0.28
k_{grz02}	Mortality rate due to grazing	0.1 day^{-1}
θ_{grz2}	Temperature dependent coefficient for grazing	1.1
f_{sc2}	Fraction of C allocated to structural purposes	0.1
W_{CChl2}	Carbon to chlorophyll ratio	65 mgC (mgChl a)$^{-1}$
QF_2	Quotient of nutrient-limited N:C ratio	0.85
W_{CN2}	Nutrient-saturated carbon to nitrogen ratio	5.67 mgC (mgN)$^{-1}$
Fall group growth, carbon to nitrogen ratios and carbon to chlorophyll ratios		
T_{opt3}	Optimal growth temperature	14 ºC
β_{13}	Temperature correction coefficient on growth rate	0.004 (ºC)$^{-2}$
β_{23}	Temperature correction coefficient on growth rate	0.006 (ºC)$^{-2}$
G_{pre3}	Gross photosynthetic rate	2.5 day^{-1}
G_{pr03}	Nutrient-saturated gross photosynthetic rate per unit light intensity	0.28 m^2(mol quanta)$^{-1}$
k_{N3}	Half saturation constant for nitrogen uptake	0.005 mg N l^{-1}
k_{RB3}	Basal respiration rate	0.03 day^{-1}
k_{RG3}	Growth-rate-dependent respiration coefficient	0.28
k_{grz03}	Mortality rate due to grazing	0.1 day^{-1}
θ_{grz3}	Temperature dependent coefficient for grazing	1.1

f_{sc3}	Fraction of C allocated to structural purposes	0.1
W_{CChl3}	Carbon to chlorophyll ratio	15 mgC (mgChl a)$^{-1}$
QF_3	Quotient of nutrient-limited N:C ratio	0.85
W_{CN3}	Nutrient-saturated carbon to nitrogen ratio	5.67 mgC (mgN)$^{-1}$

Light attenuation

k_{base}	Background light attenuation coefficient (2-D parameter)	0.16~0.6 m^{-1}
k_c	Chlorophyll self-shading coefficient	0.017 m^2(mg chl)$^{-1}$

Nitrogen regeneration, nitrification and denitrification

k_{mp}	Half saturation constant for nitrogen regeneration	0.05 mgC l^{-1}
k_{RPON}	Hydrolysis rate of RPON to RDON at 20ºC	0.008 day^{-1}
θ_{RPON}	Temperature coefficient for RPON hydrolysis	1.08
k_{LPON}	Hydrolysis rate of LPON to LDON at 20ºC	0.05 day^{-1}
θ_{LPON}	Temperature coefficient for LPON hydrolysis	1.08
k_{RDON}	Mineralization rate for RDON at 20ºC	0.008 day^{-1}
θ_{RDON}	Temperature coefficient for RDON mineralization	1.08
k_{LDON}	Mineralization rate for LDON at 20ºC	0.05 day^{-1}
θ_{LDON}	Temperature coefficient for LDON mineralization	1.08
k_{Nit}	Nitrification rate at 20ºC	0.1 day^{-1}
θ_{Nit}	Temperature coefficient for nitrification	1.08
k_{Nit_DO}	Half saturation constant of oxygen for nitrification	1.0 mgO_2 l^{-1}
k_{Denit}	Denitrification rate at 20ºC	0.05 day^{-1}
θ_{Denit}	Temperature coefficient for denitrification	1.045
k_{Denit_DO}	Half saturation constant of oxygen for denitrification	0.1 mgO_2 l^{-1}

Fraction of respired and grazed phytoplankton into organic pool

f_{RPON}	Fraction of RPON from respiration and grazing	0.15
f_{LPON}	Fraction of LPON from respiration and grazing	0.325
f_{RDON}	Fraction of RDON from respiration and grazing	0.15
f_{LDON}	Fraction of LDON from respiration and grazing	0.175
f_{nh3}	Fraction of ammonia from respiration and grazing	0.2

Exudation of phytoplankton primary productivity into dissolved organic carbon

F_{ExDOC}	Exudation fraction of primary productivity to DOC	0.1

Phytoplankton settling

V_{b1}	Base algal settling rate for winter/spring group at 20ºC	0.5 m day^{-1}
V_{N1}	Nutrient stressed algal settling rate for winter/spring group at 20ºC	1.0 m day^{-1}
V_{b2}	Base algal settling rate for summer group at 20ºC	0.3 m day^{-1}
V_{N2}	Nutrient stressed algal settling rate for summer group at 20ºC	0.7 m day^{-1}
V_{b3}	Base algal settling rate for fall group at 20ºC	0.3 m day^{-1}
V_{N3}	Nutrient stressed algal settling rate for fall group at 20ºC	1.0 m day^{-1}
θ_{sp}	Temperature correction for phytoplankton settling	1.027

Settling of particulate organic nitrogen

V_{PON}	Settling rate for PON at 20ºC	1.0 m day^{-1}
θ_{PON}	Temperature correction for PON settling	1.027

Table 2.3 Partition coefficients for organic matter in the effluent and boundary inputs

Nitrogen	***PON***	***DON***
Labile	0.5	0.5
Refractory	0.5	0.5
Phosphorus	***POP***	***DOP***
Labile	0.647	0.66
Refractory	0.353	0.33
Carbon	***POC***	***DOC***
Labile	0.4	0.2
Refractory	0.6	0.7
Reactive	-	0.05
Exudate	-	0.05

Table 2.4 Quality of data coverage for the objective interpolation

Month	Rating*
January	
February	+
March	-
April	+
May	+
June	+
July	0
August	+
September	-
October	+
November	-
December	

* Definitions of symbols: + (good), 0 (fair), - (poor).

Table 2.5 Partition coefficients of chlorophyll at the open boundary

	Winter-spring diatoms	Summer assemblages	Fall diatoms
January-April	1.0	0	0
May	0.5	0.5	0
June-July	0	1.0	0
August	0	0.5	0.5
September-November	0	0	1.0
December	0.5	0	0.5

Table 2.6 Frequencies and filtering of forcing data, validation data, and model output.

Parameters	Frequencies in the model and for validation	Frequencies of original data	Filtering	Sources
Winds	daily	hourly	no	NDBC 44013
Solar radiation	daily	hourly	no	WHOI
Boundary conditions	bi-weekly	monthly	objective interpolation	MWRA, SBNMS
River loadings	weekly	daily flow and monthly for nutrients	no	USGS
Effluent	weekly	weekly	no	MWRA
Non-MWRA effluent, CSO, Ground waters	monthly	various	"climatological" mean	Menzie-Cura, MWRA
Outfall Monitoring: Chlorophyll, nutrients and DO	12 cruises per year for nearfield 6 cruises per year for farfield	12 cruises per year for nearfield 6 cruises per year for farfield	no	MWRA
Outfall Monitoring: Primary productivity	12 samples at N04 & N18, 6 samples at F23	12 samples at N04 & N18, 6 samples at F23	no (monthly mean in Figure 3.26 & Table 3.2)	MWRA
Outfall Monitoring: Sediment fluxes	4 samples per year	4 samples per year	no	MWRA
Harbor Monitoring Program (chl, PON, DO)	weekly	weekly	no	MWRA
Model output: time series (nutrients, chlorophyll, DO)	1-day average	4 min.	no	UMB
Model output time series (primary productivity)	1-day average	4 min.	no (monthly mean in Figure 3.26 & Table 3.2)	UMB
Model output sediment fluxes	1-day average	4 min.	no	UMB

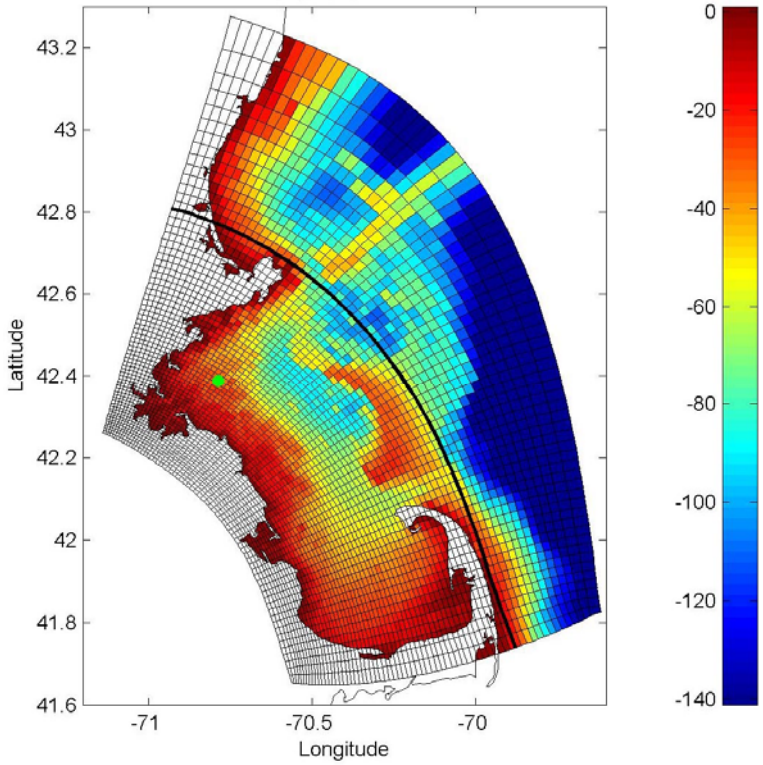

Figure 2.1. Model domain and grid in the MBS. Green dot indicates the MWRA outfall and the thick line indicates the boundary of the BEM.

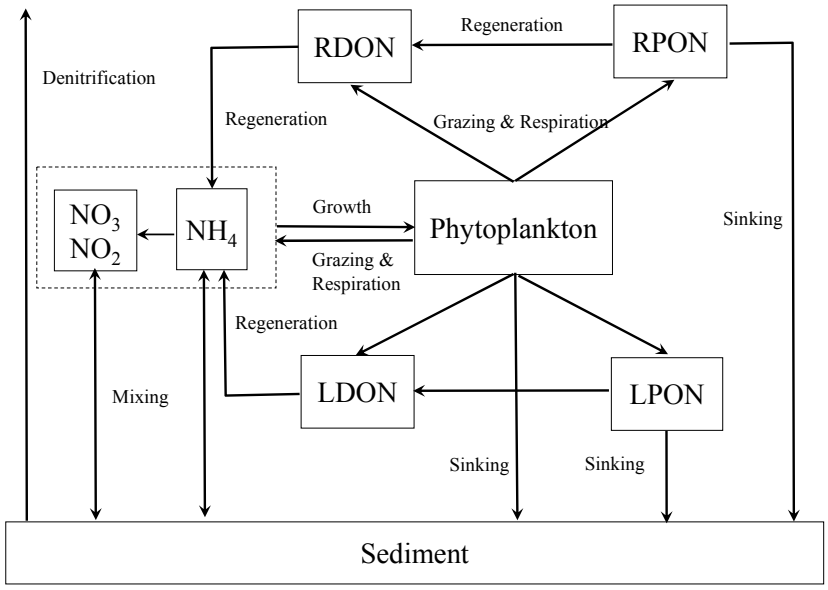

Figure 2.2. A schematic diagram for the nitrogen cycle in the BEM.

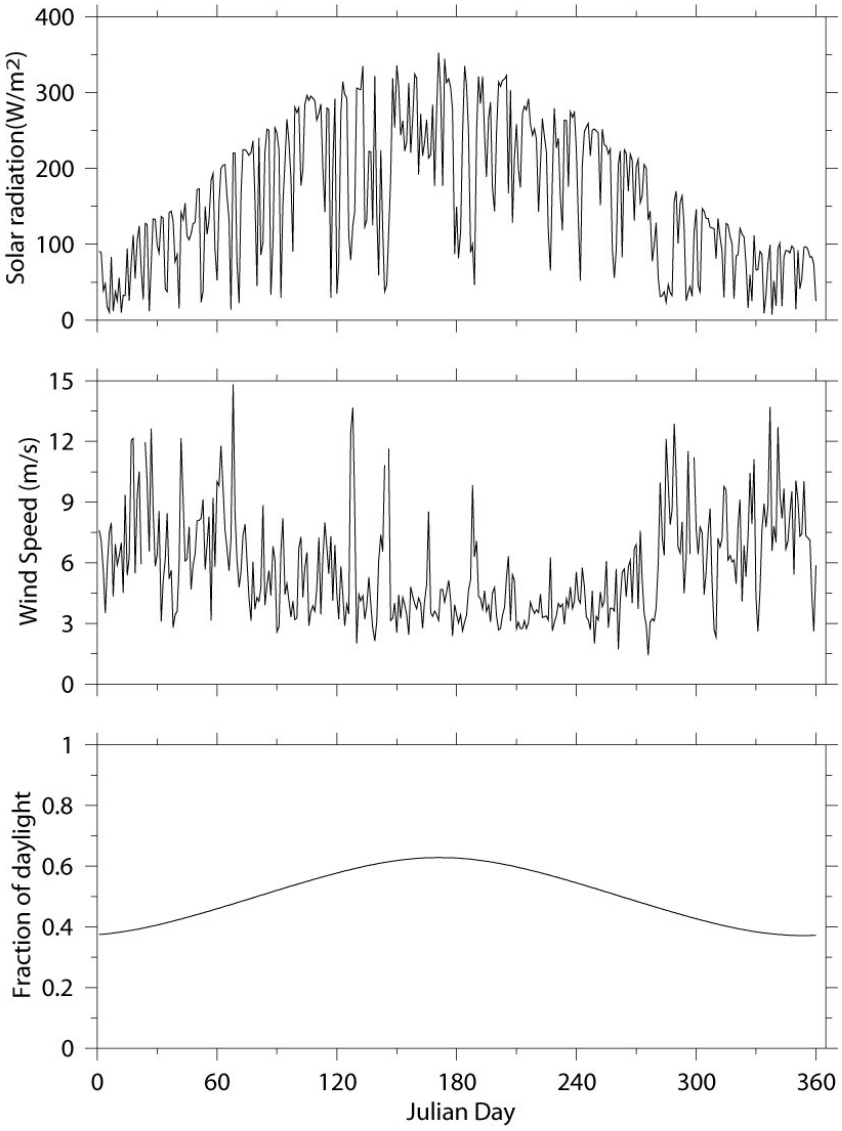

Figure 2.3. Solar radiation, wind speed, and fraction of daylight.

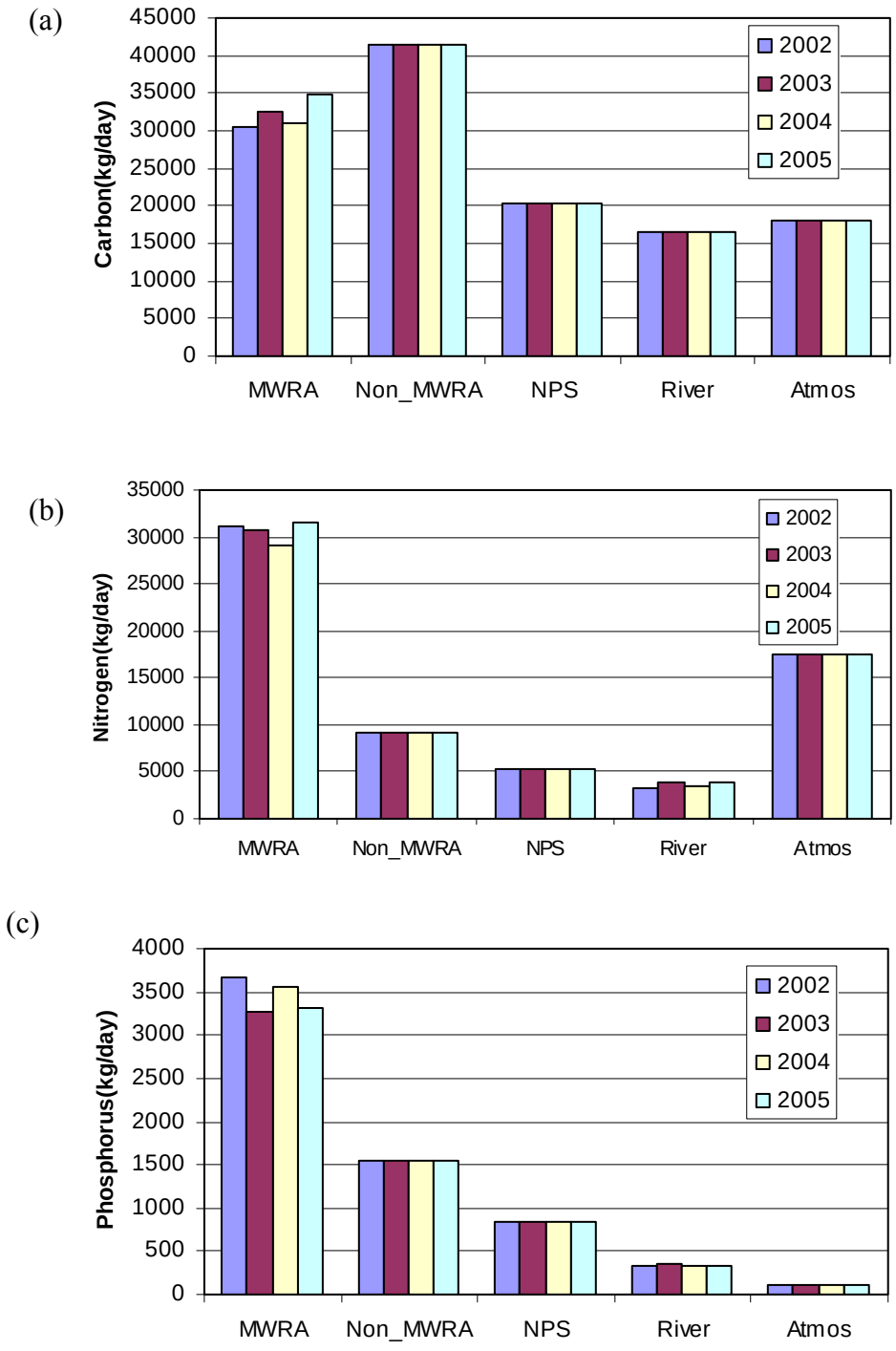

Figure 2.4. Mean daily nutrient loads for 2002-2005: (a) carbon, (b) nitrogen, and (c) phosphorus.

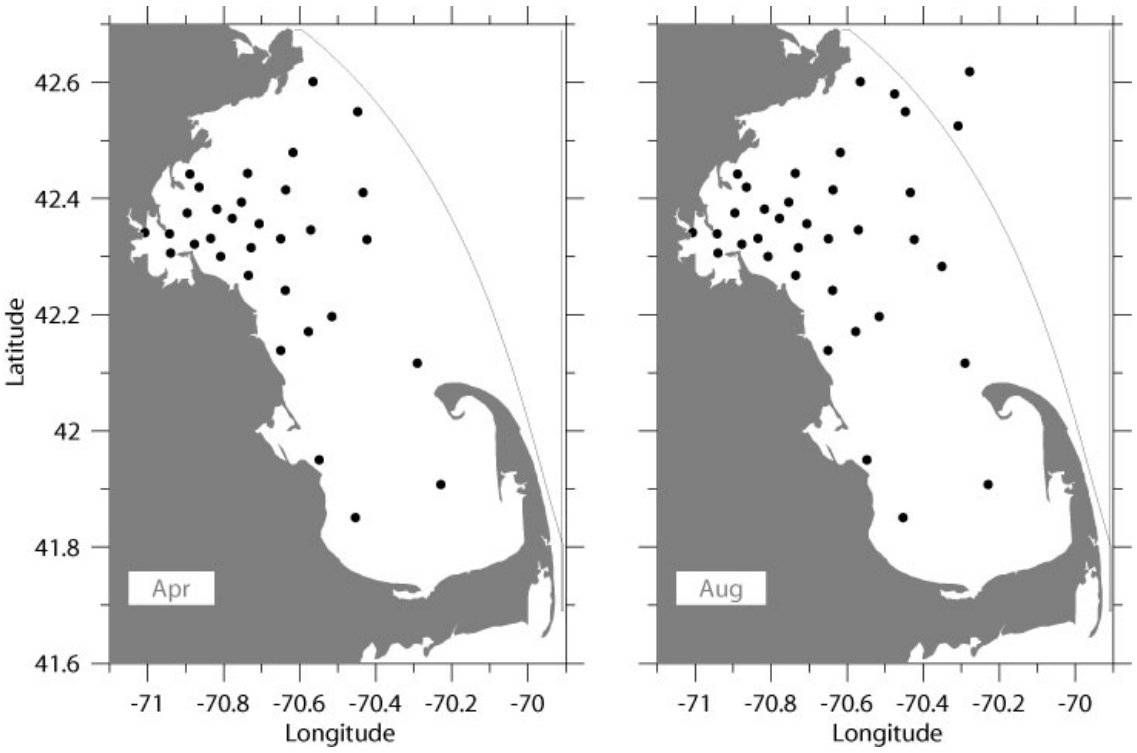

Figure 2.5. Station maps of available data in April and August.

(a)

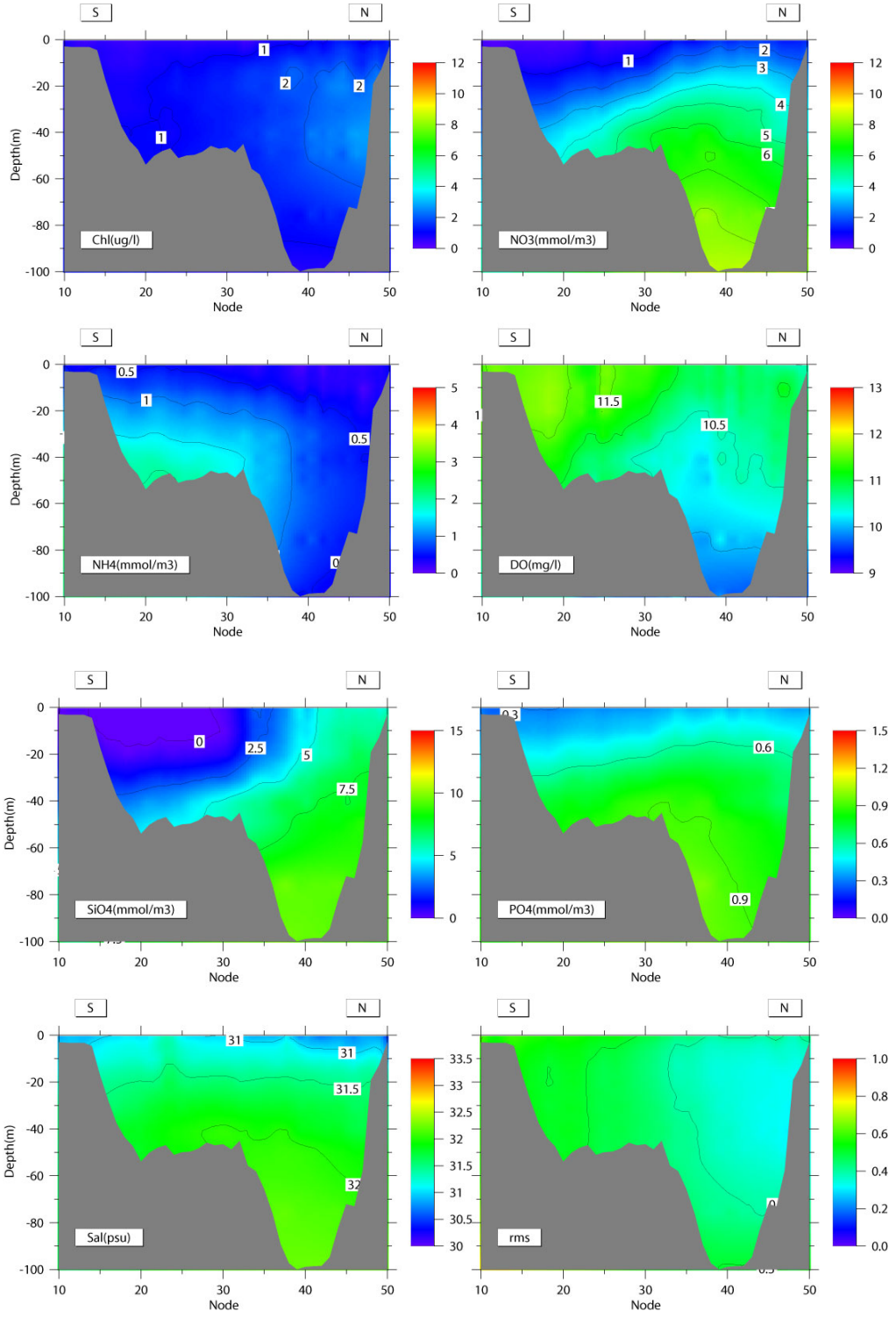

Figure 2.6. Open boundary conditions of (a) salinity, chlorophyll, nutrients, and DO, and (b) organic matter in April. The rms are also shown in the lower right panels, which apply to all of the seven parameters in (a) and (b), respectively. The node 10 indicates Cape Cod and node 50 Cape Ann. (to be continued on the next page).

(b)

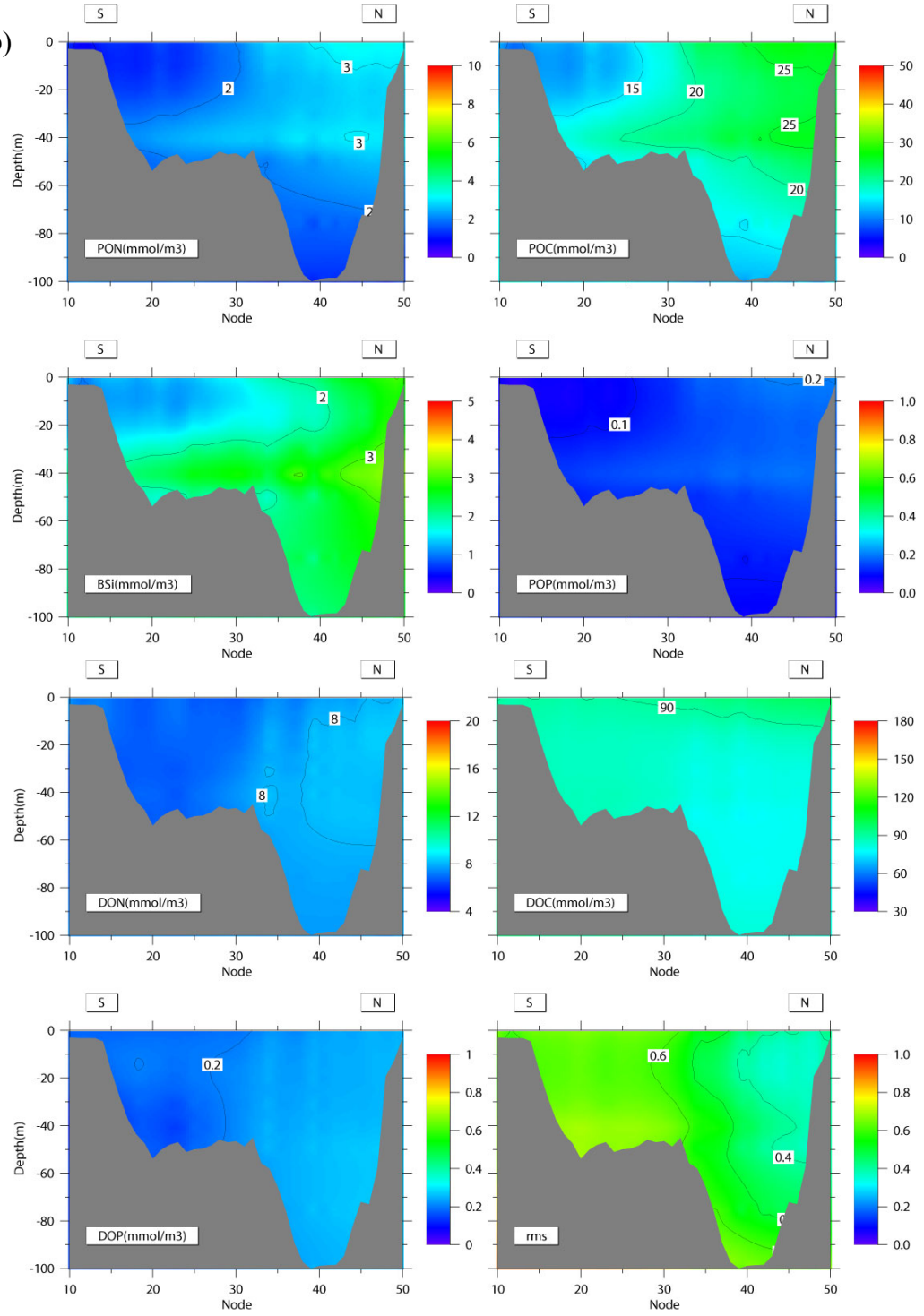

Figure 2.6. Continued.

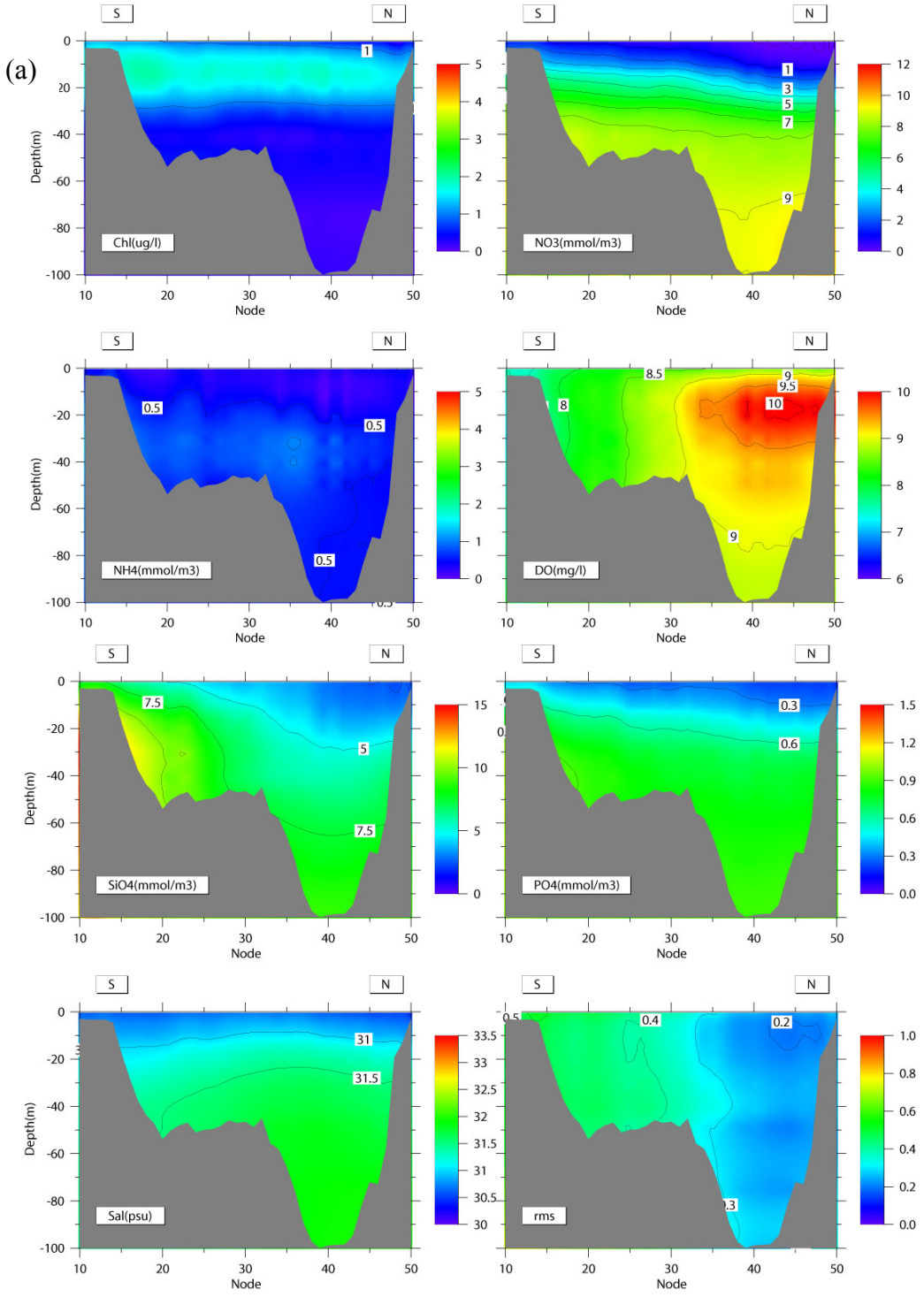

Figure 2.7. Open boundary conditions of (a) salinity, chlorophyll, nutrients, and DO, and (b) organic matter in August. The rms are also shown in the lower right panels, which apply to all of the seven parameters in (a) and (b), respectively. The node 10 indicates Cape Cod and node 50 Cape Ann. (to be continued on the next page).

(b)

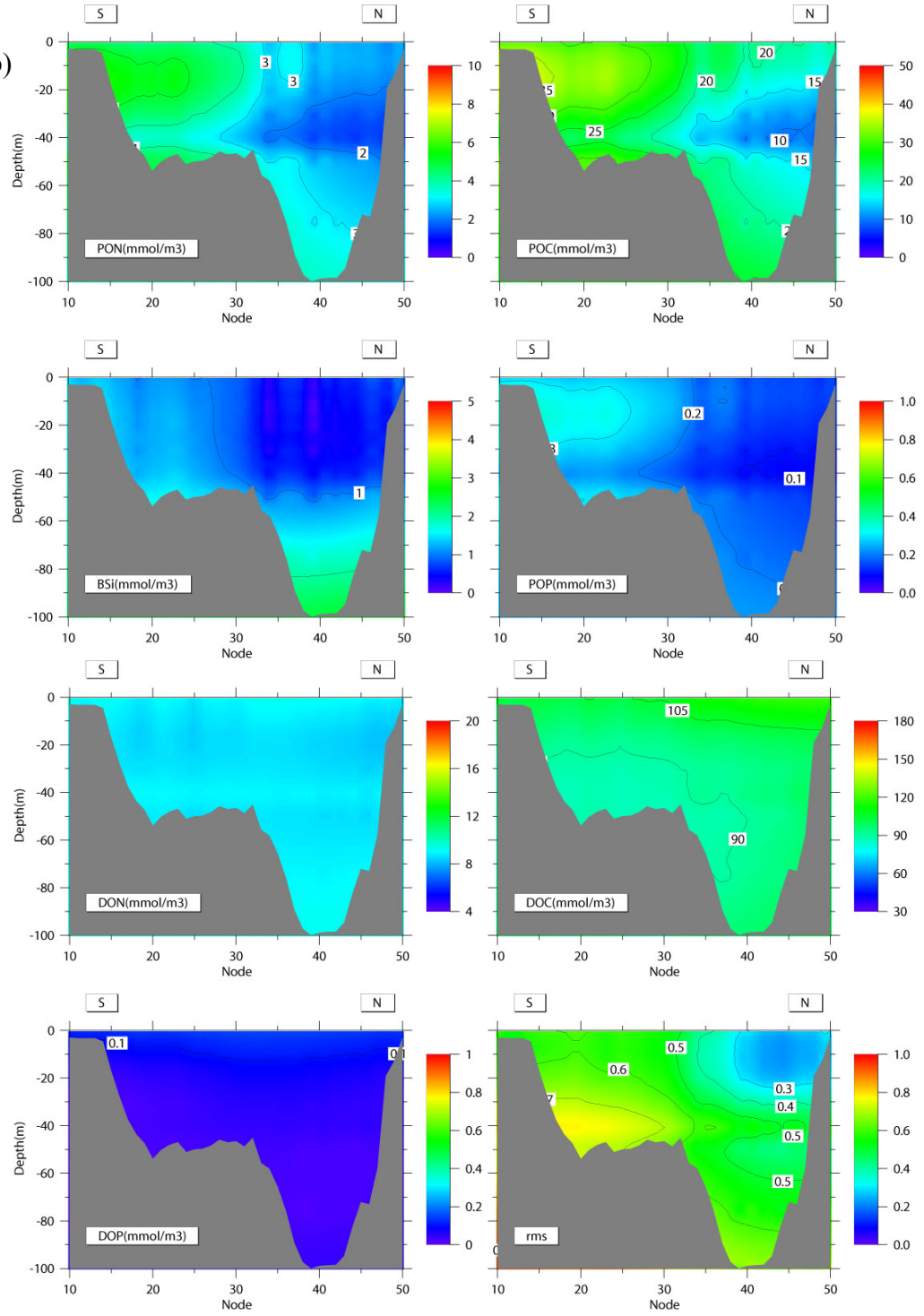

Figure 2.7. Continued.

3. VALIDATION AND DISCUSSION

3.1 Survey and data description

The hydrography and water quality in the MBS were monitored with twelve 1–day cruises per year at seven nearfield stations within 5 km from the outfall, and six 3–4 day bay–wide cruises covering the entire bay with an extra 20 farfield stations. In addition to hydrographic measurements (CTD, DO, chlorophyll fluorescence, light transmittance, and light intensity), water samples were collected at 5 pycnocline-bracketing depths to measure dissolved inorganic nutrients. A subset of those samples was analyzed for organic matter (17 stations), phytoplankton abundance (12 stations), chlorophyll, suspended solids, and DO. Primary productivity was measured at three stations: F23 close to Deer Island, and N04 and N18 within the nearfield. Detailed information about samples and data can be found in the MWRA reports (Libby et al. 2006). In this report, measurements at a subset of these stations were used for model validation (Figure 3.1a). These stations are the same stations used in the previous model validation for 2004 (Jiang and Zhou, 2006b).

The water quality in BH was also extensively monitored through the Harbor Monitoring Project (e.g., Taylor, 2004). The water quality data were collected at six stations. Among the measured variables, temperature, salinity, ammonia, chlorophyll, particulate organic nitrogen (PON) and dissolved oxygen (DO) were used for validating the results from the BEM runs.

The benthic metabolism and nutrient cycling were studied by taking sediment cores at four stations in Boston Harbor and four stations in Massachusetts Bay (Tucker et al., 2006). Fluxes of nitrate, ammonia, denitrification, dissolved silica, phosphate and SOD through the sediment and water interface were measured four times per year. Flux measurements at three stations in BH and three stations in MB were used for model validation.

3.2 Massachusetts Bay

Measured chlorophyll, DIN, PON, DON, $Si(OH)_4$, DO and DO saturation at eight chosen stations (Figure 3.1a) were used for comparison of modeled results with data in the water column. The comparisons of modeled and observed surface and bottom concentrations of these variables are shown in Figure 3.2, and the comparisons of their vertical distributions are shown in Figures 3.3-3.5.

Both modeled and observed chlorophyll concentrations exhibit a similar pronounced seasonal cycle at these stations (Figure 3.2a, and third panels in Figures 3.3-3.5). The observed chlorophyll concentrations indicated that a strong bloom occurred in late February and early March. The water column was still well-mixed and chlorophyll was evenly distributed in the upper 40m during the bloom. The observed chlorophyll concentrations were generally low in the summer except for some episodic high values. A moderate fall bloom occurred in late September with chlorophyll concentrations about 2-4 μg/l except the high values at N04. Comparing to observations, the BEM reproduced the overall seasonal cycle with a strong spring bloom in the first half of March 2005 and moderate surface chlorophyll values in the summer. However, the model over-predicted the fall bloom and summer bottom chlorophyll concentrations.

Observed DIN showed a typical seasonal cycle with concentrations higher than 10 μM in the winter and lower than 3 μM since mid-March consistent with the chlorophyll cycle of lower productivity in the winter and high productivity in the spring bloom (Figure 3.2b, second panels in Figures 3.3-3.5). The surface DIN was depleted from May to September, and increased from September to the end of 2005. The bottom DIN concentrations increased after June and remained high the rest of the year except at F23 where DIN was depleted between May and September.

Modeled DIN concentrations agree with observed ones except that modeled bottom DIN concentrations were lower than the observed during the spring (Figure 3.2b). The model reproduced the seasonal pattern of the nitrogen cycling including strong biological uptake during blooms and regeneration in the late spring and summer.

Observed $Si(OH)_4$ concentrations showed a similar seasonal cycle as that of the DIN concentrations except that the surface $Si(OH)_4$ was not depleted in the summer, suggesting a nitrogen limitation to phytoplankton in this area (Figure 3.2c). Overall, modeled $Si(OH)_4$ agreed with data at all stations.

The other two nitrogen pools, PON and DON, are compared in Figures 3.2d and 3.2e, respectively. Here PON includes both non-living and living particulate organic nitrogen. Both modeled and observed PON and DON concentrations showed a weak seasonal variability with relatively low PON concentrations in the late summer associated with low production and high regeneration. Modeled surface PON, surface DON and bottom DON agreed with observed data, while bottom PON concentrations were over-predicted by 2~3 fold most of the year. Similarly, model POC (including both phytoplankton and particulate organic nitrogen). Model surface POC also agrees with data, while the model over-estimates the bottom POC, mostly during the second half of the year (Figure 3.2f).

The comparisons between modeled and observed DO concentrations are shown in Figure 3.2g and Figures 3.3-3.5. Similar to other years, observed DO concentrations in 2005 exhibited a strong seasonal cycle at all stations. Both of the surface and bottom DO concentrations increased in the winter and early spring due to deep mixing produced by surface cooling and wind stirring, and enhanced primary production. The observed DO peaked in February at the shallow coastal stations (N10, F01, and F23) and in late March at offshore stations, and decreased steadily throughout the late spring and summer, primarily due to the decrease of saturation DO, which has an inverse relationship with water column temperature. Surface DO concentrations reached their minima in September and then increased slightly from October to December. The increase was slower than that in normal years, which may be explained by the moderate winds in November and December 2005 (Figure 2.3). At inshore stations, bottom DO reached their minima in late summer (August-September), whereas at offshore stations, it decreased throughout the spring, summer and well into November. Normally, the bottom DO would rebound in late September or early October (e.g., Jiang and Zhou, 2004b, 2006b).

Overall, the model reproduced the seasonal cycle of observed DO concentrations with some differences. First, at inshore stations, the model DO concentrations peaked about 2-3 weeks later than the observed. Secondly, the model did not reproduce the high DO values observed at some stations during the August cruise. The model's inability in simulating episodic high DO events has been reported during previous simulations (e.g. Jiang and Zhou, 2006b).

The comparisons of modeled and observed saturation of DO are shown in Figure 3.2h, which indicated a pronounced seasonal cycle at these stations. Based on observations, the surface DO saturation was highest in the mid-summer and lowest in the winter except at N07, where the highest DO saturation was observed in early April. The surface waters were generally saturated in oxygen in all seasons and appear to be 110~120% oversaturated in the late spring and the entire summer. The DO oversaturation in surface waters was mostly due to photosynthesis. Similar to other years, the bottom DO saturation peaked in the spring and then decreased until October at inshore stations and until November at offshore stations. Bottom waters were generally undersaturated in oxygen. The model reproduced the seasonal cycle of DO saturation, and the modeled values generally agreed with the observed except those at N04 and N07 during the spring period.

3.3 Boston Harbor

The six stations chosen for comparison represent North Harbor (024, 130 and 140) and South Harbor (077, 141 and 124), respectively (Figure 3.1b). Measured temperature, salinity, ammonia, chlorophyll, PON and DO concentrations were compared with the modeled values at these stations (Figure 3.6).

It is clear that temperature in the harbor showed little spatial gradient throughout the year and modeled temperature values agreed with the observed ones. Salinity in the harbor showed a clear gradient with the lowest salinity found at 024 and 140, two stations within the Charles River and Neponset River plumes, respectively. Salinity was lowest in April and May and also low in late October and November due to high river flows. Modeled salinity values generally agreed with observed ones, though the model was

unable to produce stronger vertical salinity gradients in the river mouth during the peak flow in April-May and October-November, especially at station 140.

Observed ammonia in the North Harbor has little seasonality, and is primarily influenced by the variability in river flows and ammonia concentrations. In the South Harbor, observed ammonia concentrations were high in winter and nearly depleted in summer. Modeled ammonia showed a similar pattern; it generally agreed with observed in the South Harbor but differed with data in the North Harbor, likely due to the lack of adequate forcing data for the river. Modeled NH_4 concentrations were generally higher than the observed in the winter (December, January, and February).

Observed chlorophyll in the harbor indicated a dramatically different seasonal cycle from those in MB with a strong spring bloom in March and relatively high values in the late spring and summer (Figure 3.6d). Consistent with these, the observed PON concentrations showed a narrow strong peak in February and a broad peak in the summer (Figure 3.6e). The DO concentration increased in the winter, peaked in February, decreased continuously in the spring and summer, reached a minimum in August and September, and then increased again throughout the rest of the year (Figure 3.6f).

Modeled chlorophyll and PON predicted the observed ones except those in the late summer and fall. Modeled DO concentrations predicted a similar seasonal cycle as the observed, but were generally higher than the observed in the summer by 1~2 mg/l, which was likely due to the over-predicted summer bloom.

3.4 Primary productivity

The comparison of vertically integrated primary production (PP) between modeled and observed values is shown in Figure 3.7. The observed PP at stations N04 and N18 showed a seasonal cycle consistent with observed chlorophyll concentrations: a spring bloom in late February and a fall bloom in August-September. At station F23, limited measurements showed a weak seasonality.

The modeled PP at both N04 and N18 generally agreed with observed data except that the model over-predicted primary production in the summer. At F23, the modeled

PP agreed with all measurements, but the overall curve was above the measured. This suggests that modeled PP may be over-estimated, a problem that had been encountered during earlier simulations (HydroQual, 2000; HydroQual, 2003; Jiang and Zhou, 2004b, 2006b).

3.5 Sediment fluxes

The model performance in simulating the coupling between the water column and sediment is validated through fluxes of nitrate (JNO_3), ammonia (JNH_4), silicate (JSi), phosphate (JPO_4), SOD, and denitrification (JN_2) (Figure 3.8).

In BH, the model reproduced the observed seasonal trends of all parameters but the peaks were generally delayed and over-predicted as compared to data, except for denitrification. The over-prediction was likely due to over-predicted production in the summer months as seen in chlorophyll and PON (Figure 3.6). Model denitrification was lower than the observed, which may be due to higher DO simulated.

In MB, the modeled fluxes agreed well with most observed values at all stations. A weak seasonal pattern increasing fluxes from March to September could be identified in most modeled fluxes, which were not present in observed fluxes. The model under-estimated the silicate fluxes at station MB05.

3.6 Statistical analysis

In order to quantitatively evaluate the agreements and differences between modeled and observed results, a regression analysis was carried out for key biogeochemical variables. Correlation coefficients (r) and rms of the differences between modeled and observed salinity, chlorophyll, DO, DIN, and silicate at all sampled stations and depth-integrated primary production at N04 and N18 were computed. The rms is used to quantify the mean differences between modeled and observed values for each parameter. The results are summarized in Table 3.1 and the correlations of a subset of the parameters are shown in Figures 3.9. All correlations are significant with $p<0.01$. Modeled and observed chlorophyll concentrations have a significant correlation (r=0.31), though

modeled chlorophyll concentrations had much smaller variations than the observed which were reported in previous simulations (Jiang and Zhou, 2004b, 2006b).

Modeled and observed surface and bottom DIN have good correlations with regression slopes of 1:1. Modeled silicate concentrations at both surface and bottom had good correlations with observed values (r=0.79). Modeled and observed nutrient concentrations at the lower end of concentrations were less scattered, which suggested that the model was able to capture the major nutrient drawdown by phytoplankton, though modeled chlorophyll values showed substantial deviations from the observed values.

Modeled and observed DO concentrations correlated very well, having rms values less than 0.6 mg/l, the best regression lines following 1:1 ratio, and correlation coefficients higher than 0.94 at both the surface and bottom. Overall, bottom DO concentrations in 2005 were higher than for average years.

The correlation between modeled and observed PP is shown in Figure 3.10. Similar to previous reports, the observed PP were interpolated over the year to derive monthly mean values (excluding January since there was no observation in January), and modeled results were averaged to derive monthly means for N04 and N18 (total 22 data points). The results at F23 were not used because only 6 measurements were made. These results indicated that the modeled PP had significant correlations with the observed values (p<0.05), similar to the regression results of chlorophyll.

Table 3.1. Summary of correlations between modeled and observed results*.

Variables	Surface		Bottom	
	Correlation coefficient (r)	RMS	Correlation coefficient (r)	RMS
Salinity	0.77	0.63	0.87	0.4
Chlorophyll	0.31	2.3	0.39	2.2
DO	0.92	0.6	0.94	0.5
DIN	0.87	2.2	0.59	3.0
$Si(OH)_4$	0.79	2.7	0.67	3.0

* The number of samples n=234 for each parameter.

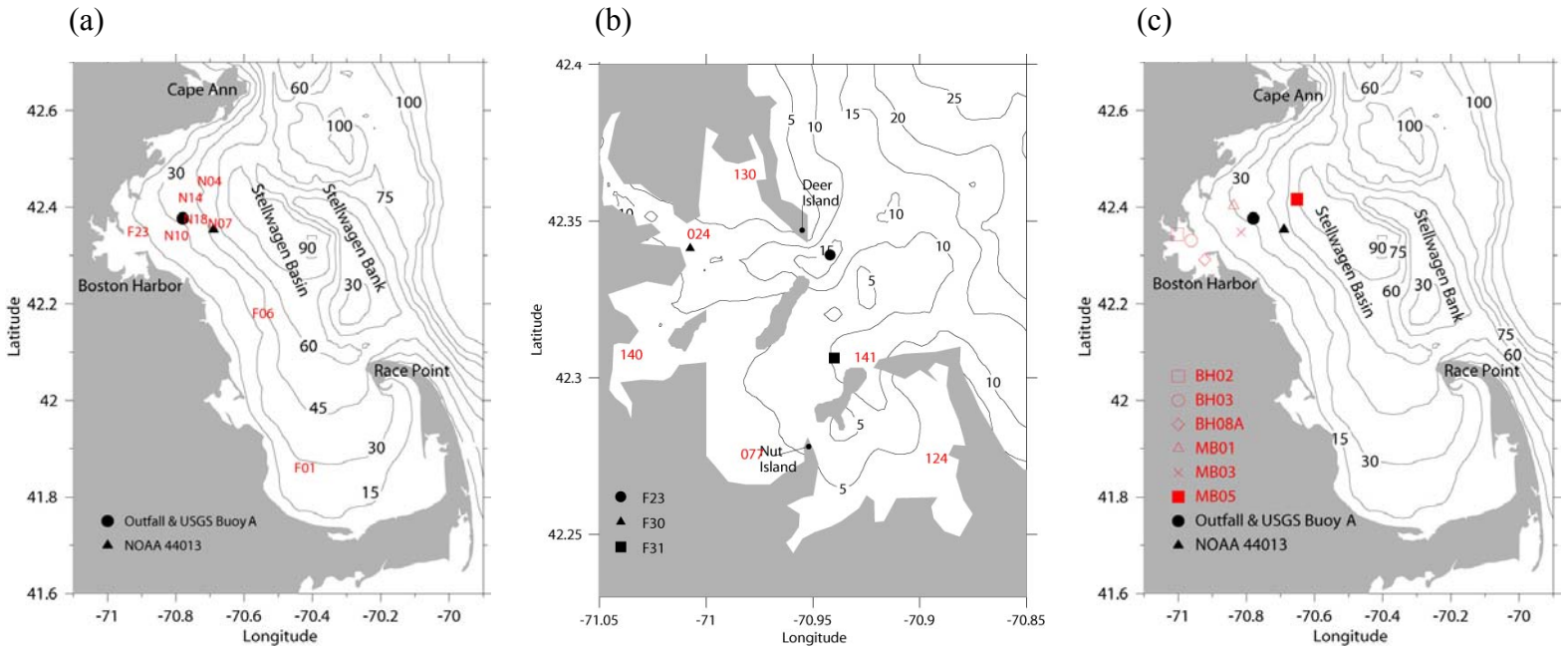

Figure 3.1 Station maps for data comparison: (a) MB, (b) BH, and (c) stations for sediment fluxes. The station N18 was only used for primary production comparison.

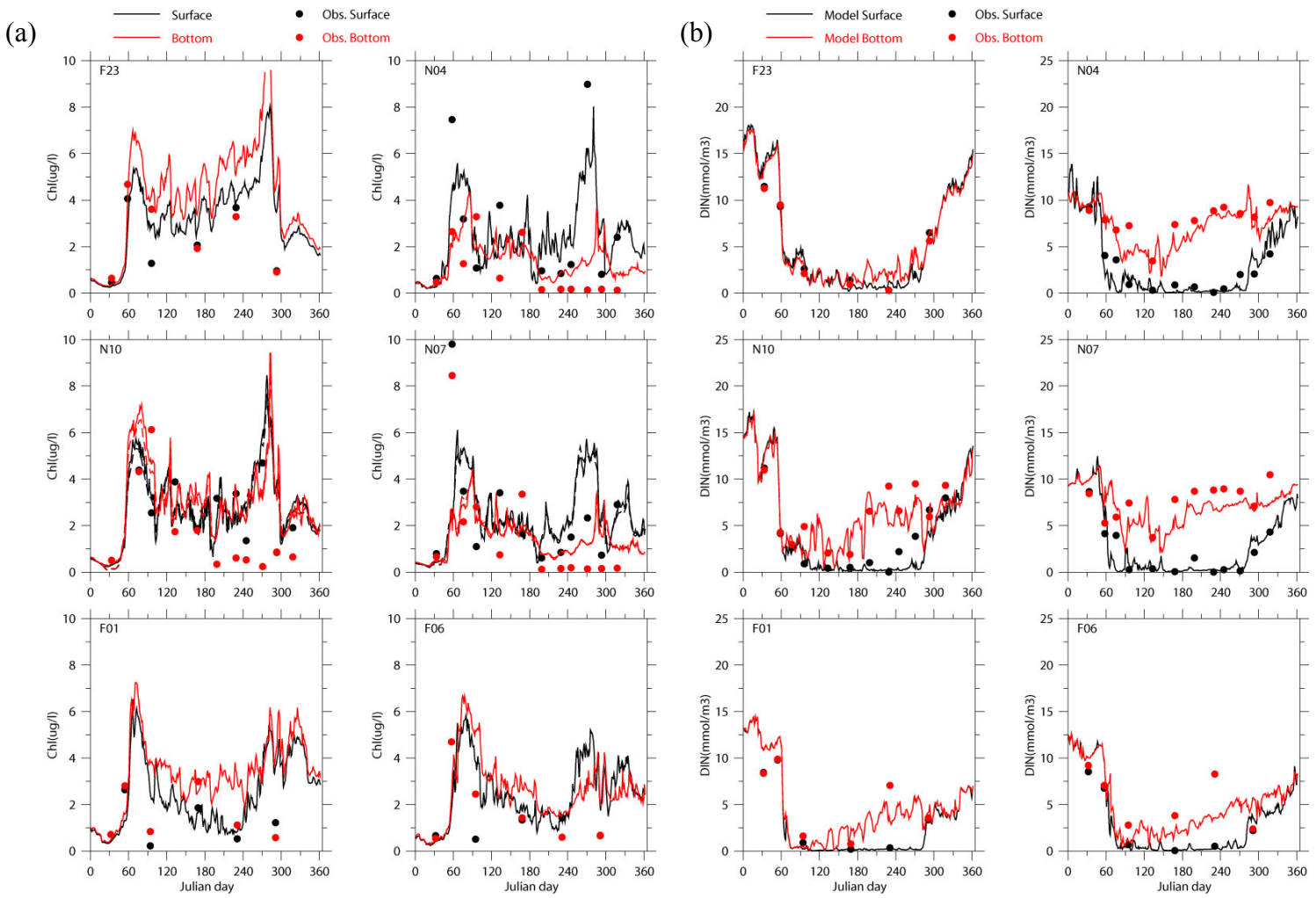

Figure 3.2. Time series of modeled and observed variables: (a) chlorophyll, (b) DIN, (c) SiO_4, (d) PON, (e) DON, (f) POC, (g) DO, and (h) DO saturation (to be continued on next page).

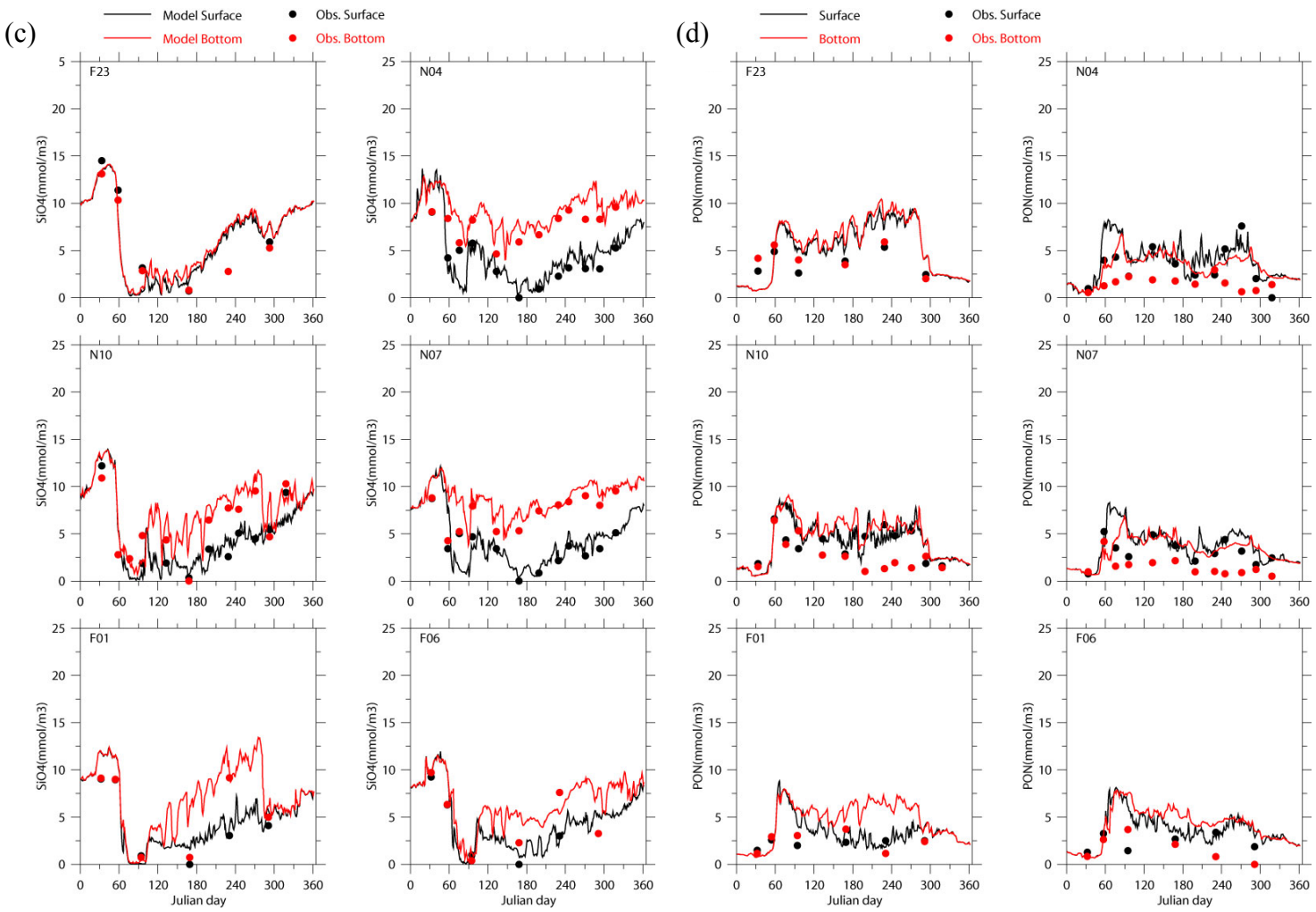

Figure 3.2. Continued.

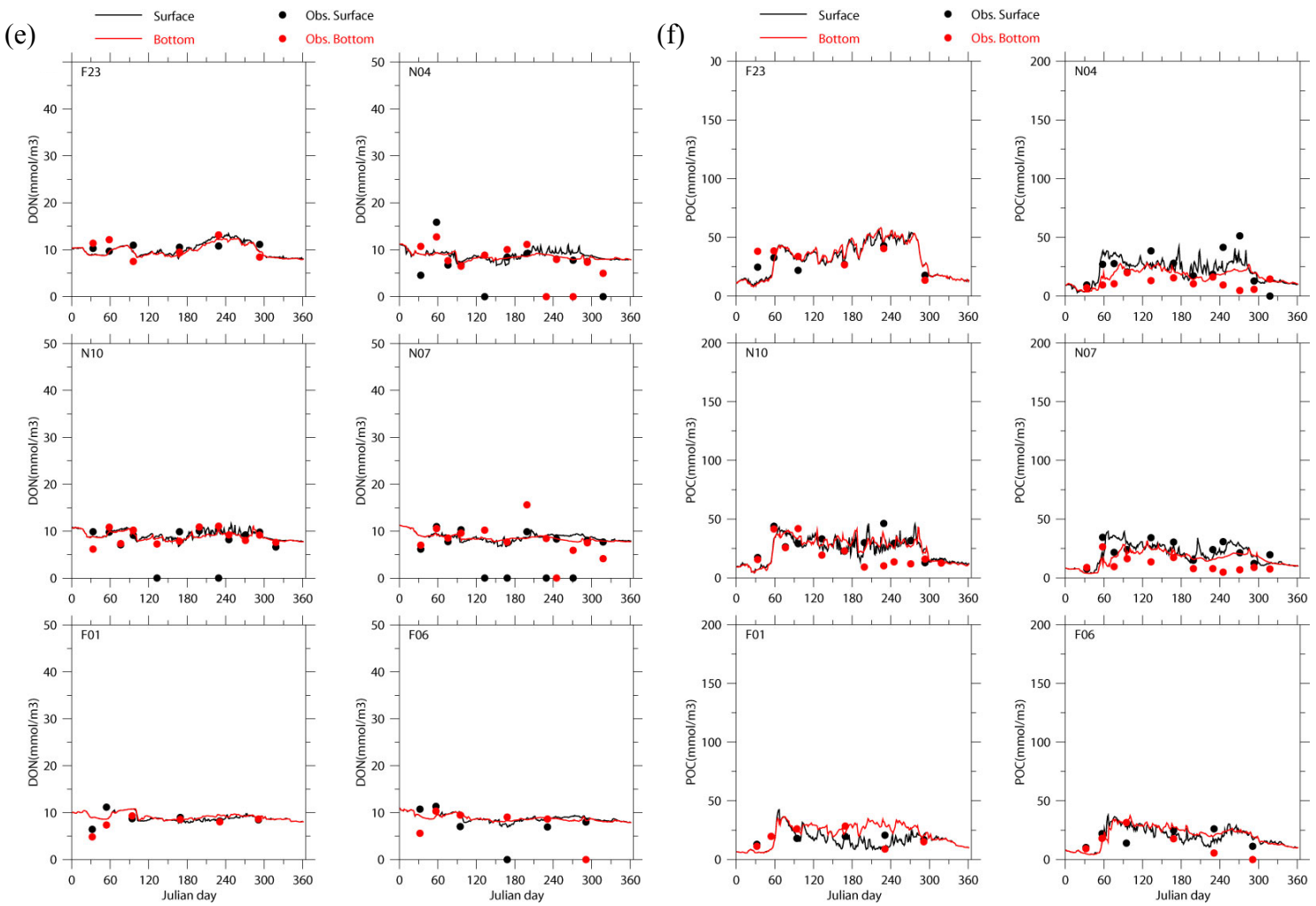

Figure 3.2. Continued.

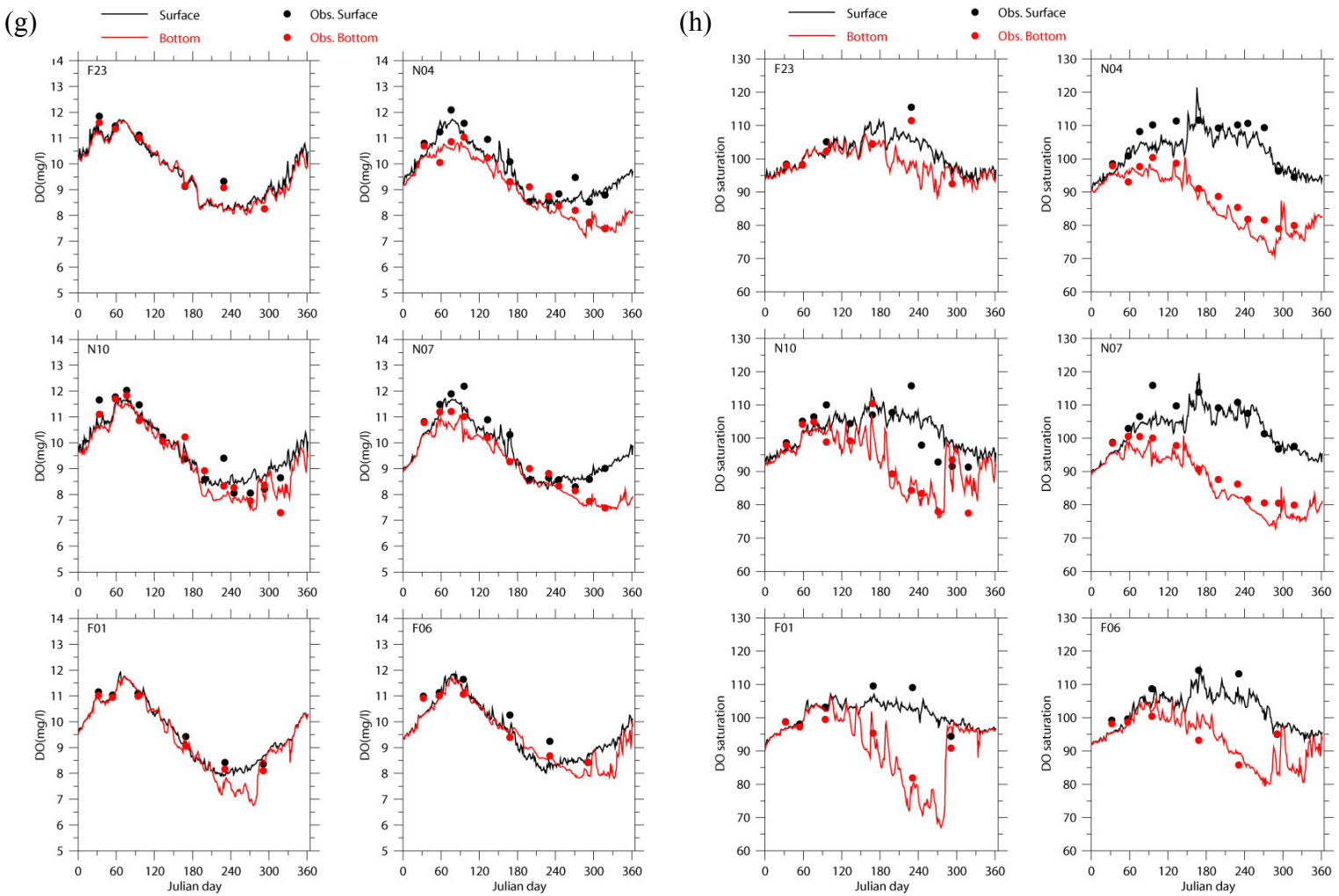

Figure 3.2. Continued.

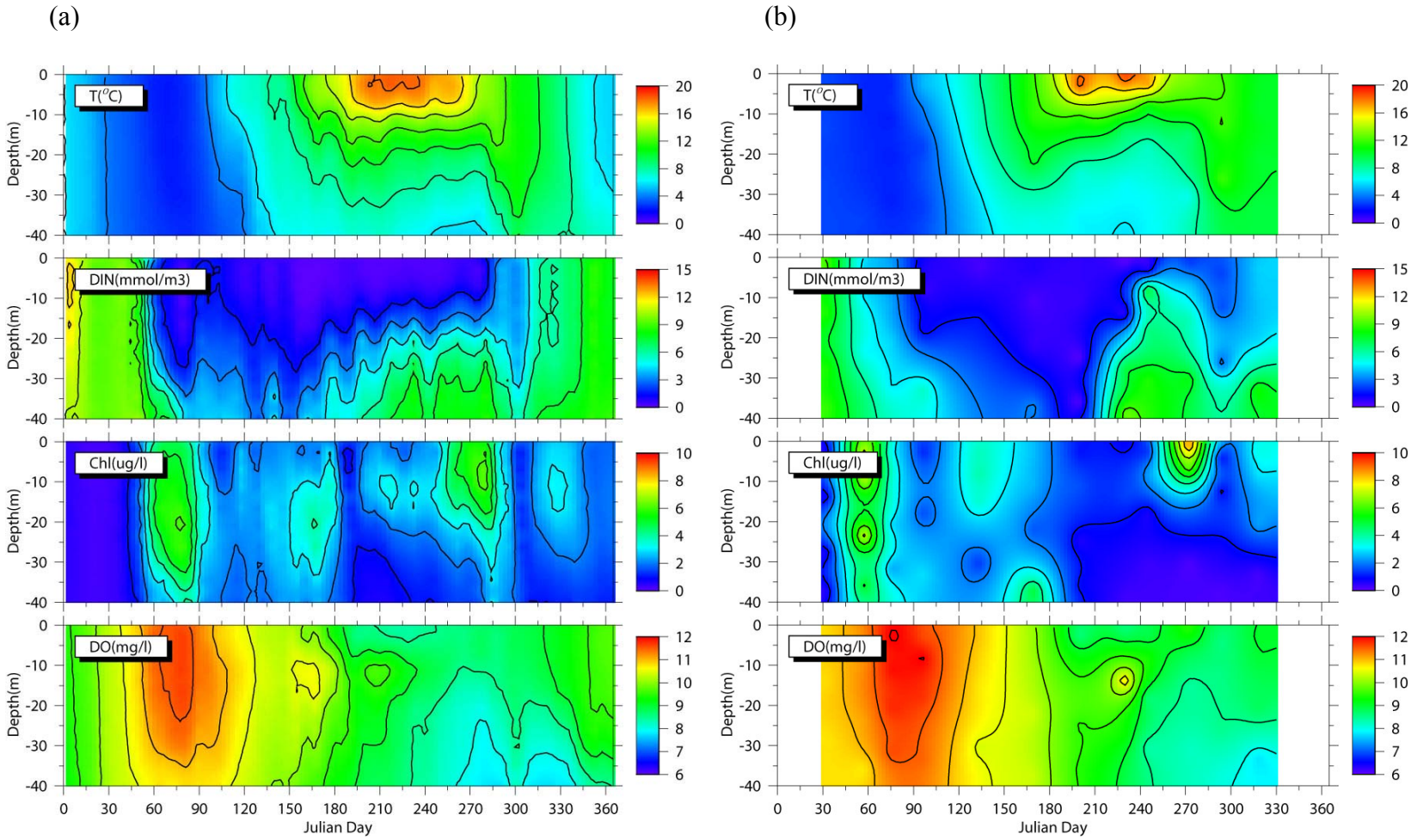

Figure 3.3. Time series of (a) modeled and (b) observed vertical distributions of temperature, DIN, Chl and DO at station N04.

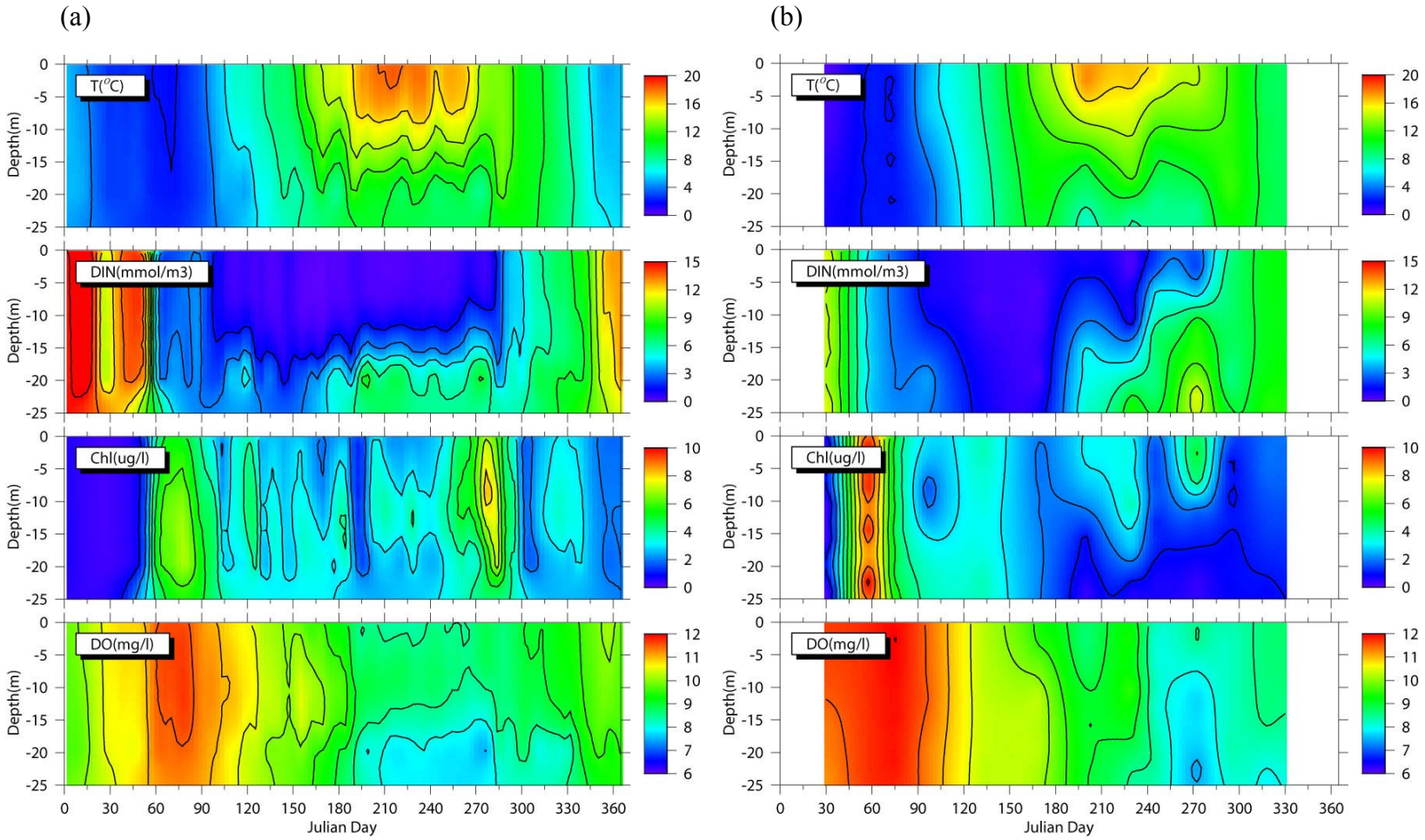

Figure 3.4. Time series of (a) modeled and (b) observed vertical distributions of temperature, DIN, Chl and DO at station N10.

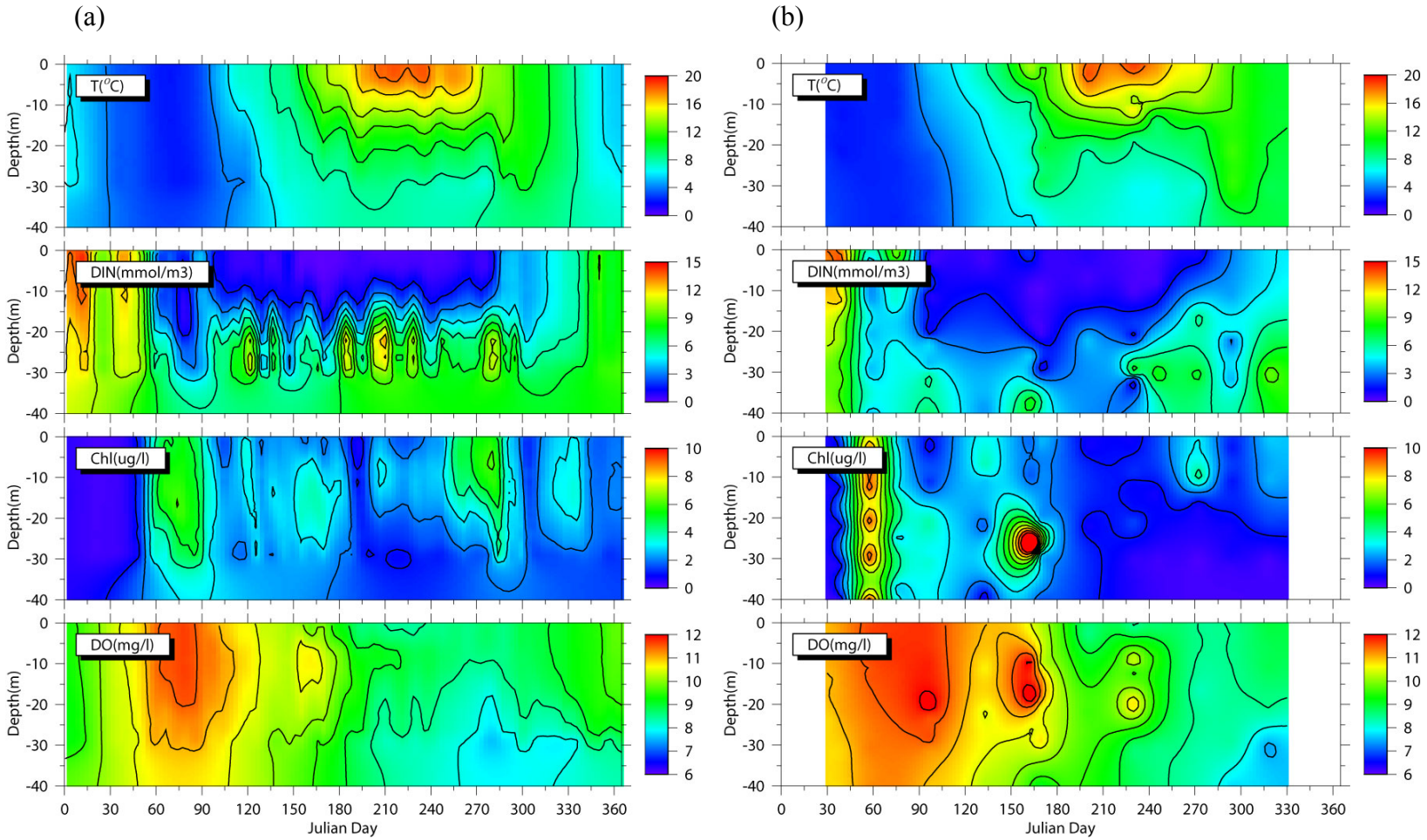

Figure 3.5. Time series of (a) modeled and (b) observed vertical distributions of temperature, DIN, Chl and DO at station N16.

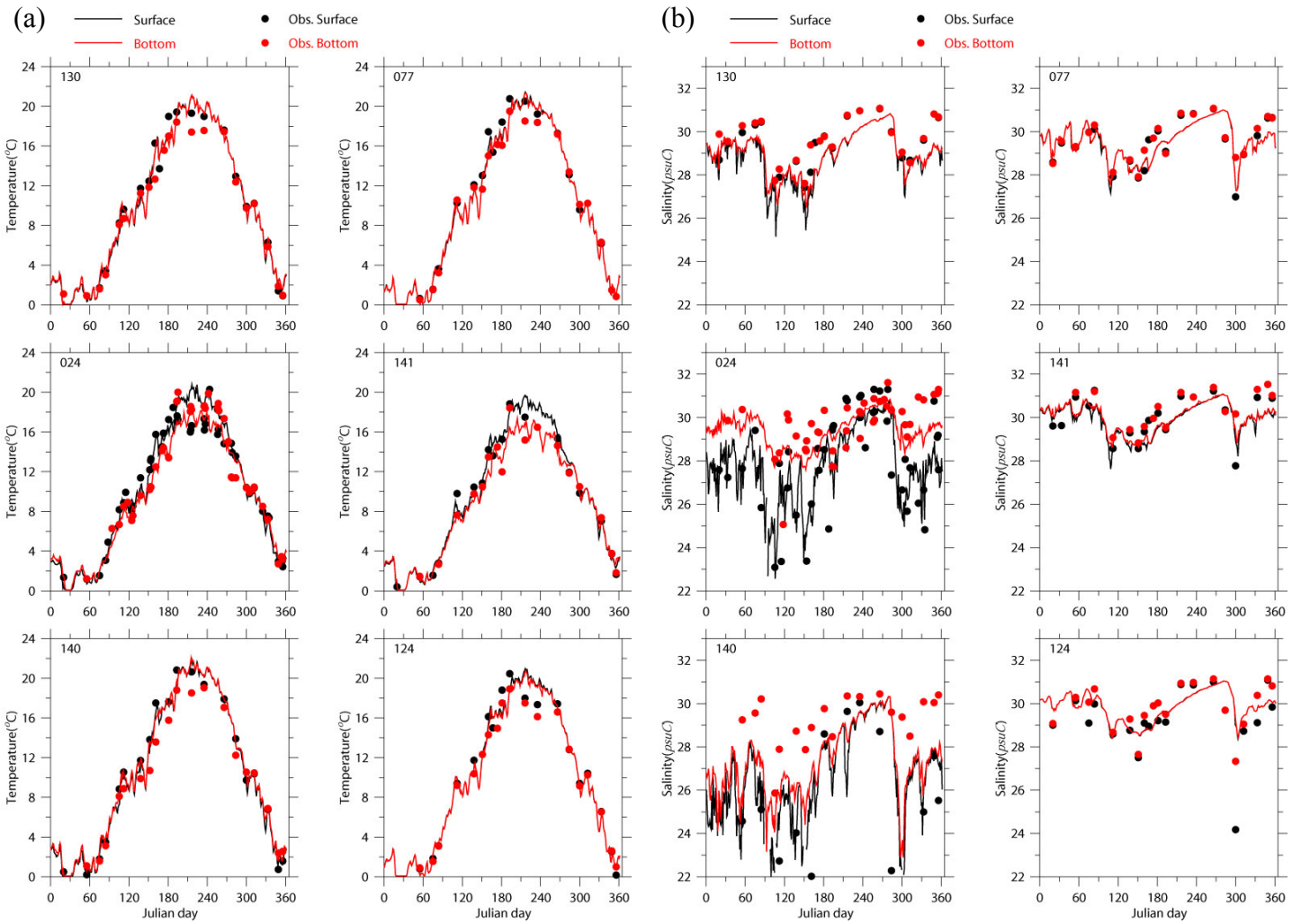

Figure 3.6. Time series of modeled and observed (a) Temperature, (b) Salinity, (c) NH_4, (c) chlorophyll, (e) PON and (f) DO in BH
(To be continued on next page).

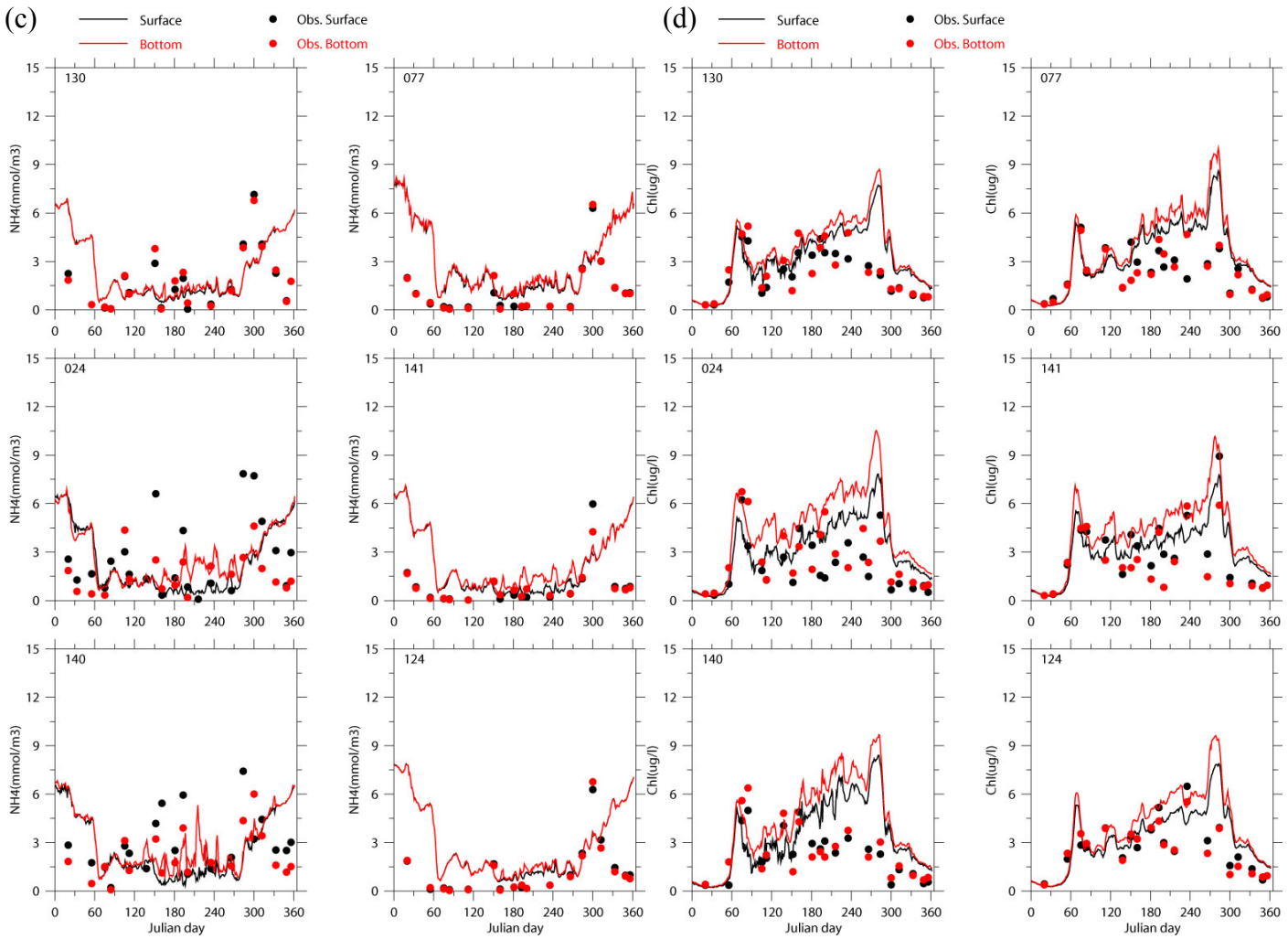

Figure 3.6 Continued.

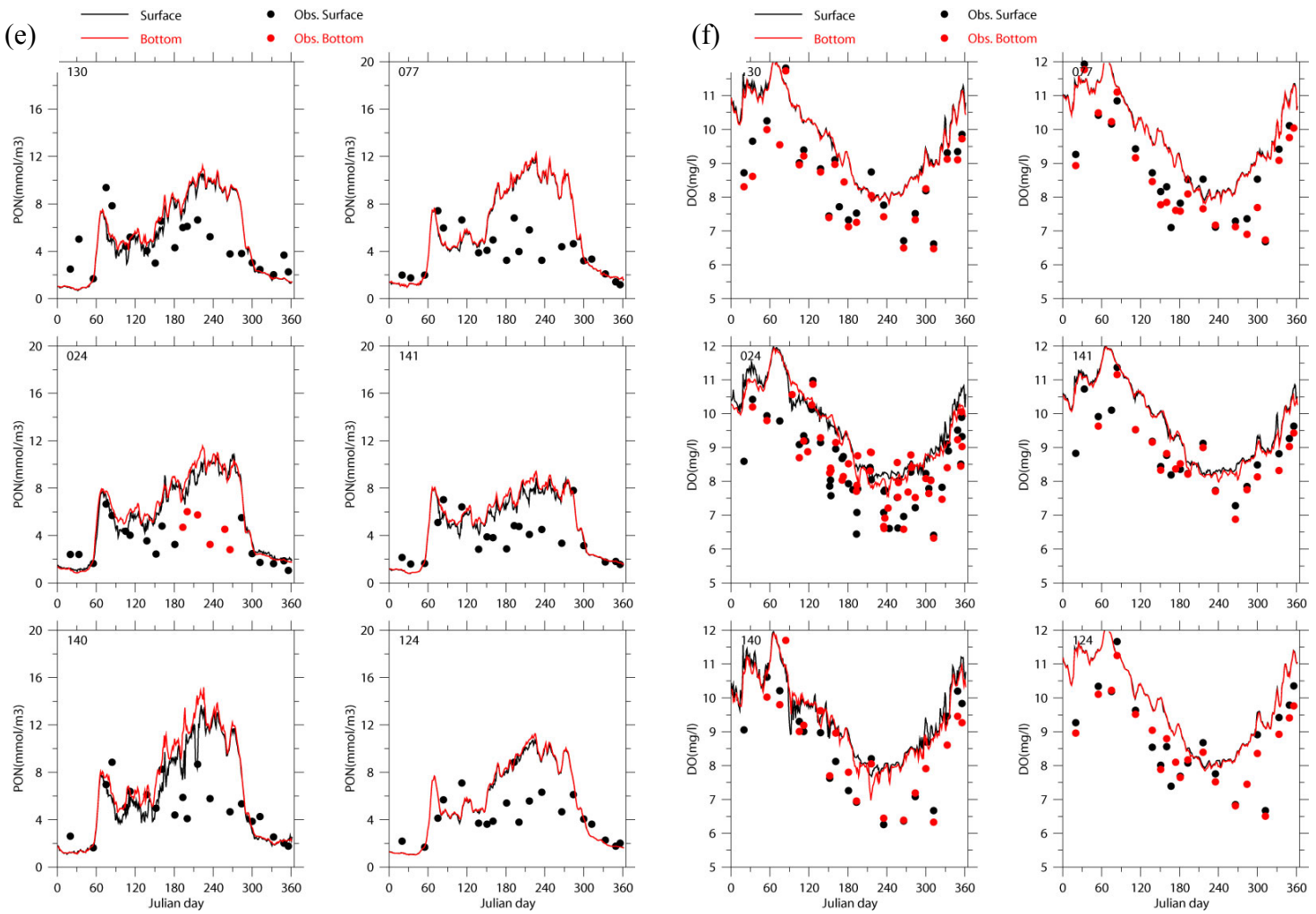

Figure 3.6. Continued.

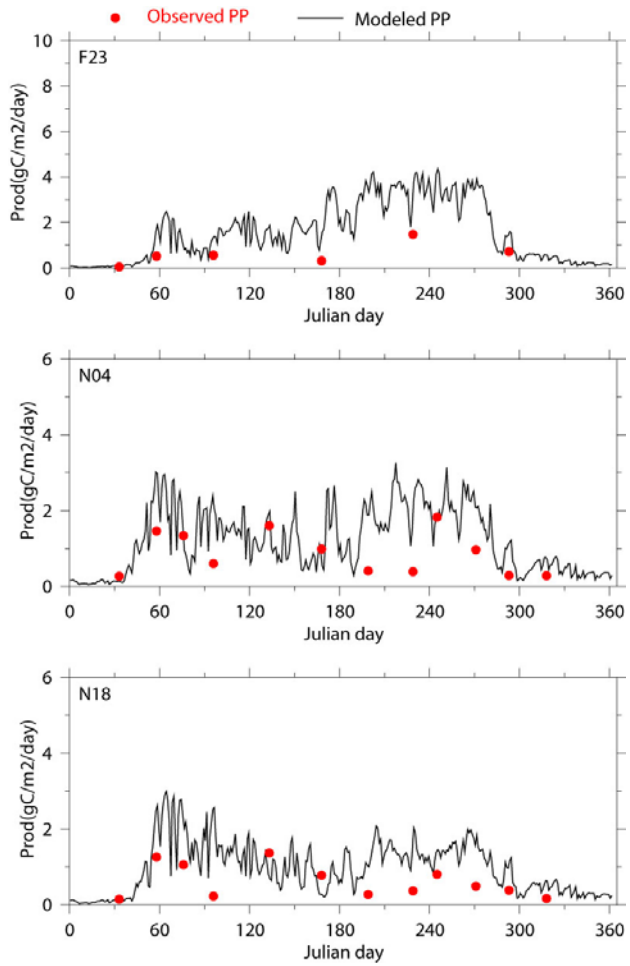

Figure 3.7. Modeled and observed primary production (PP).

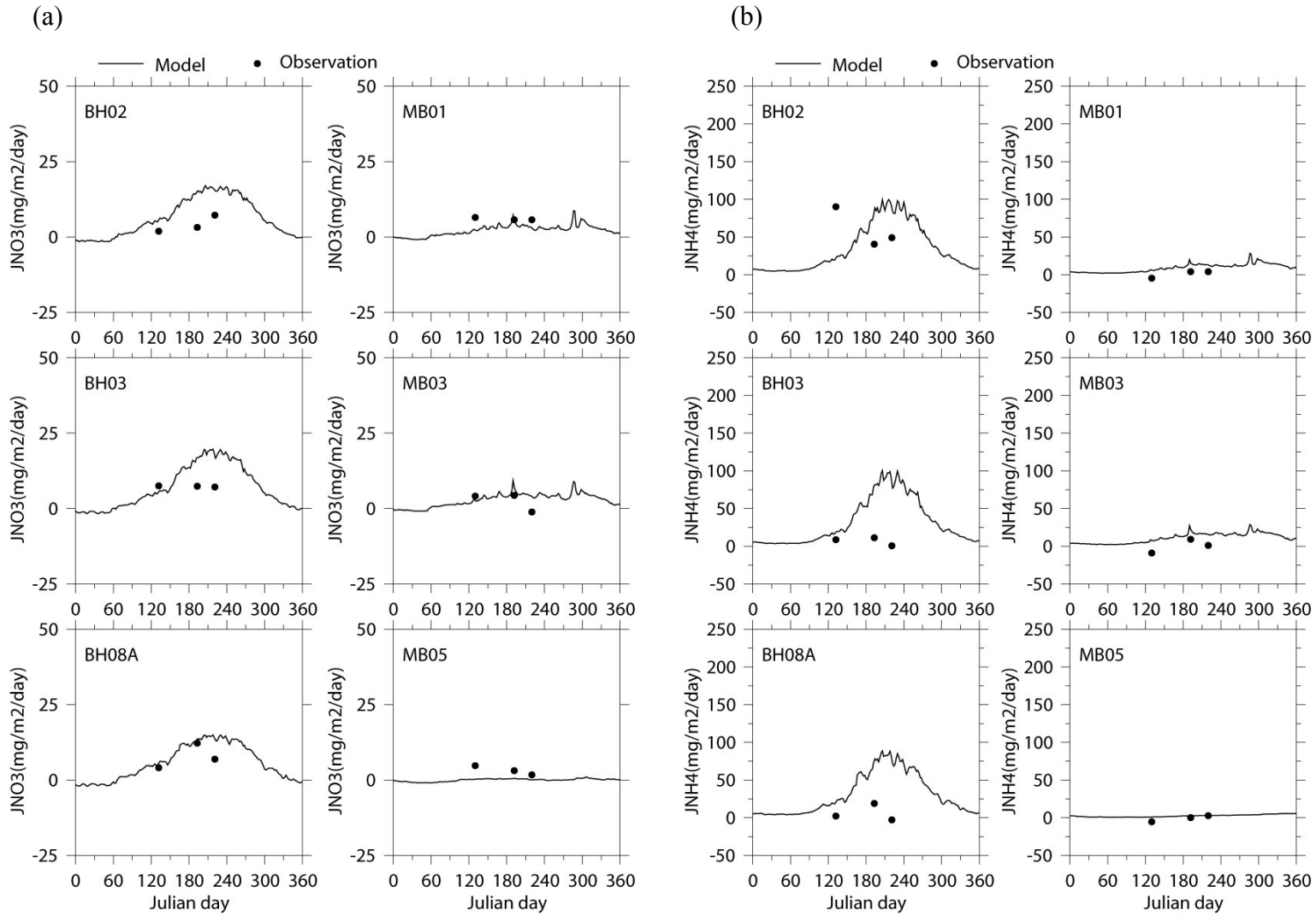

Figure 3.8. Nutrient fluxes and sediment oxygen demand in 2002: (a) JNO_3, (b) JNH_4, (c) JSi, (d) JPO_4, (e) SOD and (f) JN_2. (To be continued on next page).

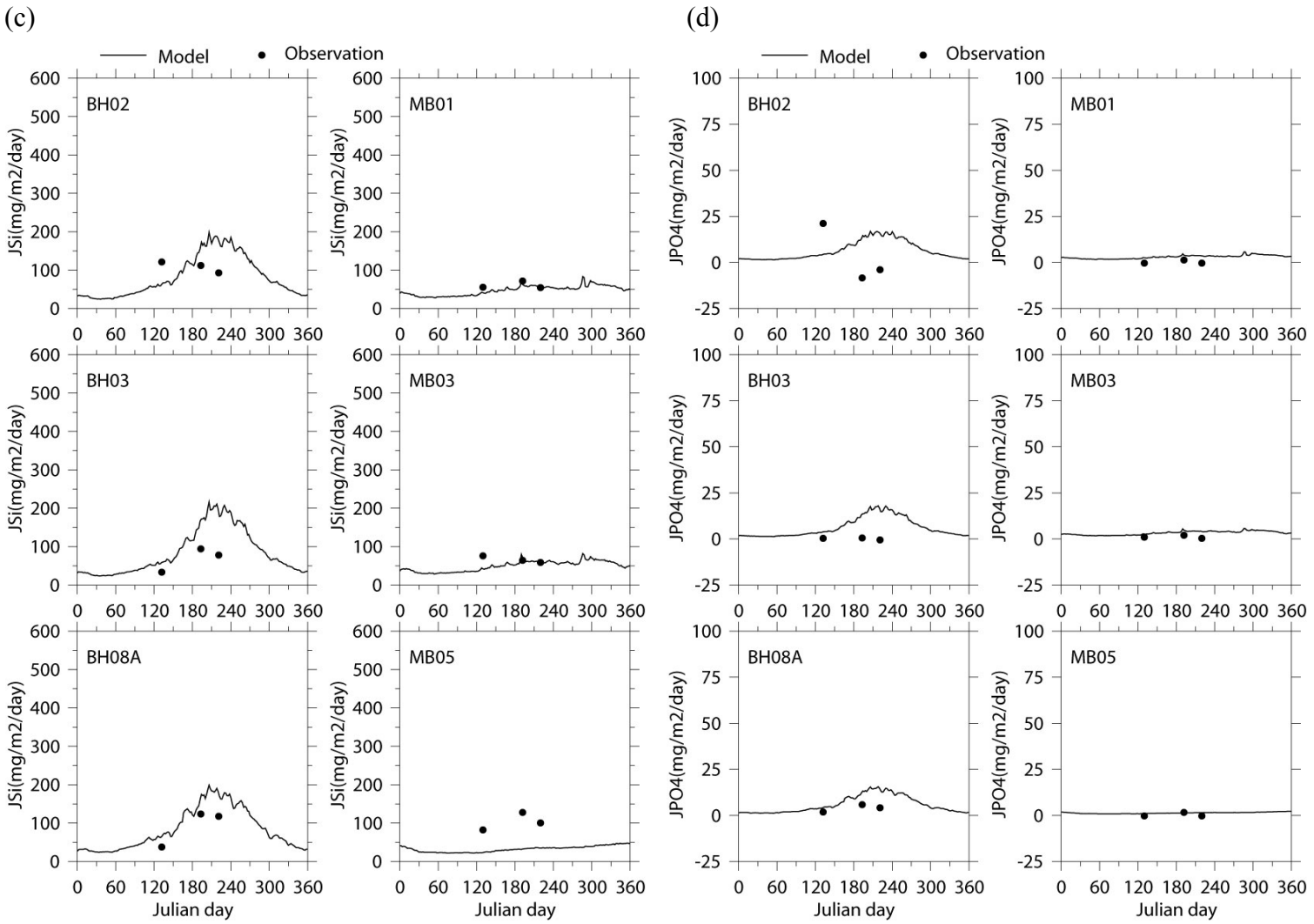

Figure 3.8. Continued.

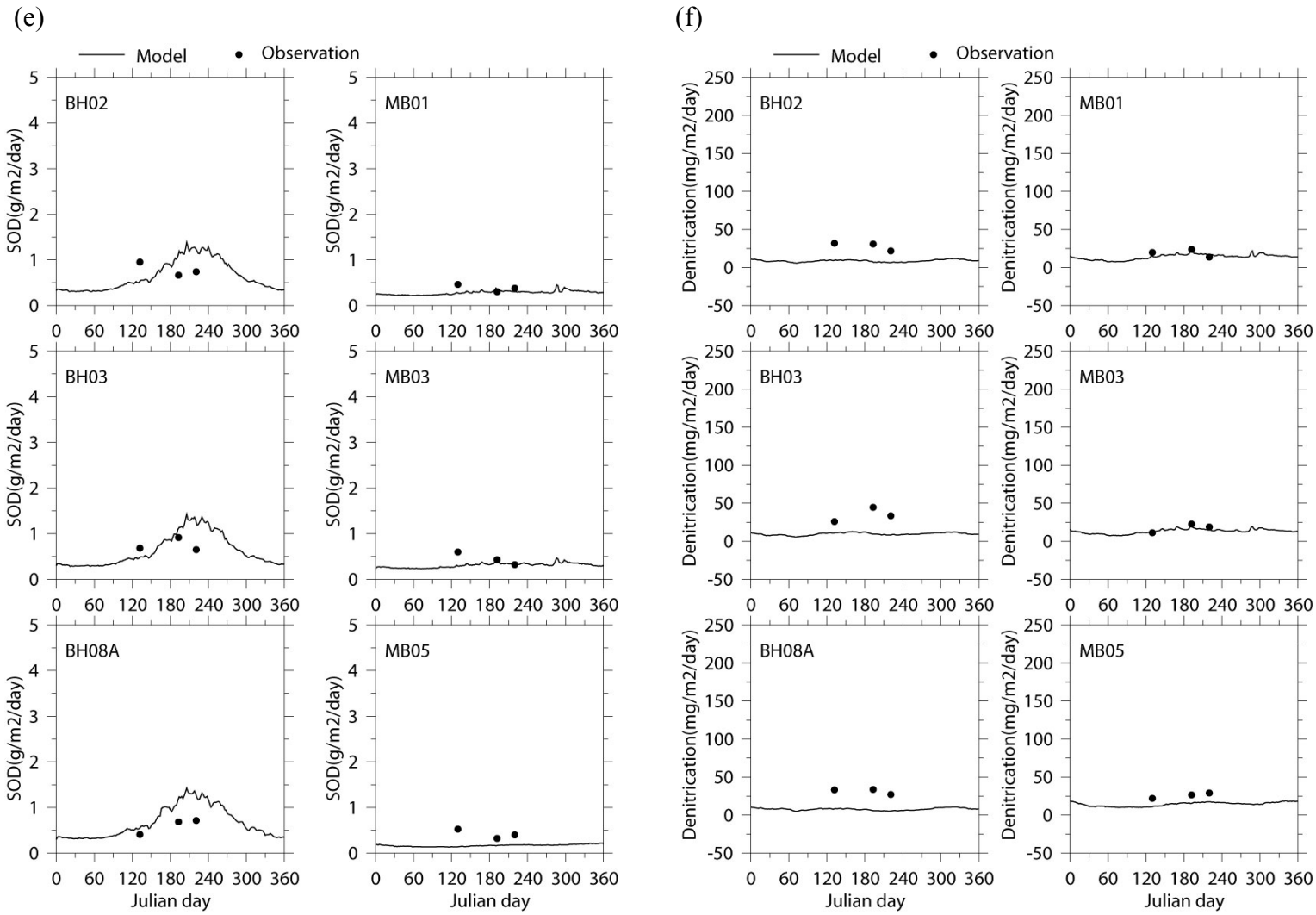

Figure 3.8. Continued.

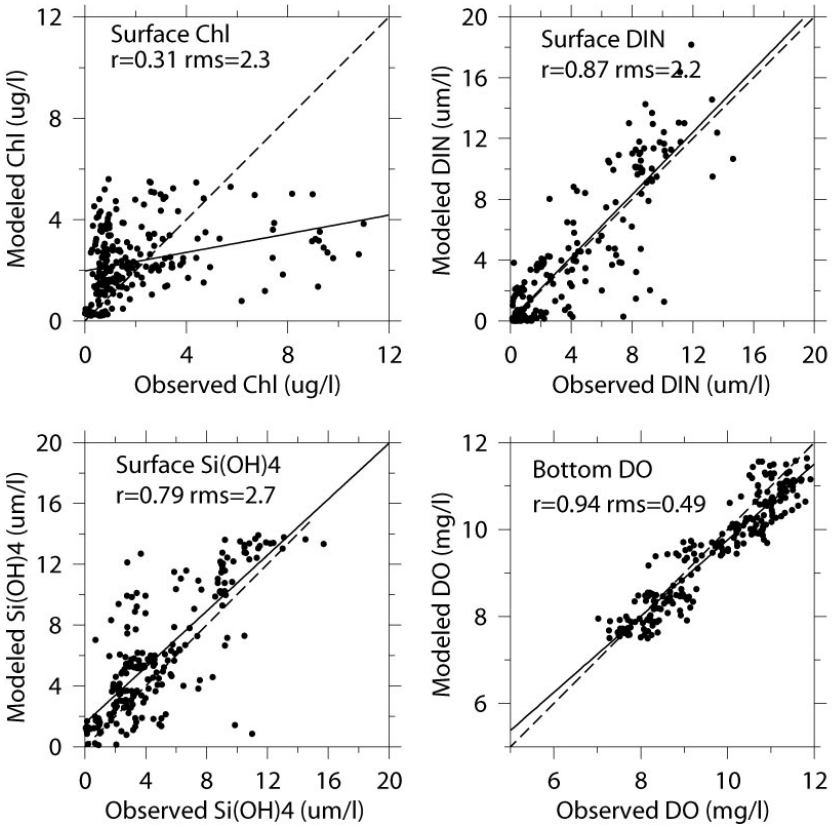

Figure 3.9. Correlation between modeled and observed concentrations for key parameters. Solid lines indicate best linear fit and dash lines indicate 1:1 relationship. Also shown are the correlations coefficients (r) and root-mean-square (rms).

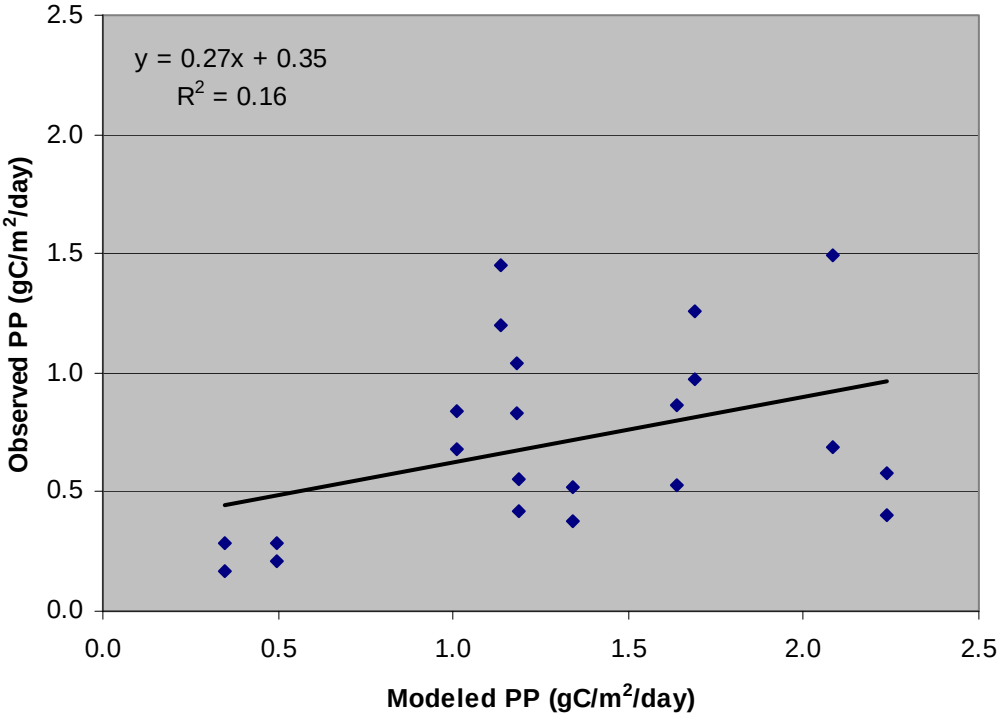

Figure 3.10. Correlations between modeled and observed primary productivity (PP). Also shown are the best linear fits (solid line) and the value of R^2.

4. POTENTIAL OUTFALL EFFECTS ON ALGAL BLOOM

This section analyzes the potential outfall effects on phytoplankton blooms in the MBS. It also examines the specific effects of outfall on phytoplankton blooms during the period of May 2005 with two nor'easter events and massive red-tide blooms in the western GOM coast and MBS (Anderson et al. 2007; Libby et al. 2006). A simple nutrient budget is computed to examine the role of nutrient loadings, especially that added by storms during that period.

4.1 Seasonal patterns of effluent impacts

In order to examine the effect of the outfall effluent, two numerical experiments were conducted: (1) a control experiment include all nutrient sources (Control), and (2) an experiment by setting nutrient concentrations in the effluent to zero (NOS). The differences of key values were computed: Control minus NOS model runs. The maps of monthly means (Figures 4.1-4.4) and time series of box averages over a domain covering the majority of the MBS (Figures 4.5-4.8) are presented here.

The modeled patterns of DIN differences are consistent with those of earlier modeling studies using a passive tracer in a hydrodynamic model (Signell et al. 2000), using a coarse resolution version of the water quality model (HydroQual, 1995), and using the present model for 2001 model run (Jiang and Zhou, 2006b). The results show a strong seasonal variability of DIN in coastal regions with little influence in the deep basin. Chlorophyll differences in both the magnitude and spatial coverage also show a strong seasonality with the lowest in the winter, the highest in the spring, and only limited to BH and the northwestern coast in the summer and fall.

In the winter, the DIN differences were the highest (Figures 4.1 and 4.7). Spatially, the DIN in the effluent was transported by the coastal currents along the western coast, forming a narrow and long band (width <10km) extending from the outfall to Plymouth Harbor. The effluent could also be found in CCB though with the mean DIN differences less than 1 μM. The effluent contributed less than 10% of the DIN in the winter but contributed little to chlorophyll (Figure 4.8).

In the spring, the water column in the MBS was weakly stratified so that the maximum DIN difference was near the bottom within 5 km near the outfall. The deep

DIN differences outcropped at the surface in BH and an area between the outfall, Hull, and Scituate (Figure 4.2). During this period, the outfall effluent contribution to the bottom DIN was largest in terms of percentage for the year, which was around 10-20% (Figure 4.8). The surface chlorophyll differences were generally distributed south of the outfall without a clear pattern; the bottom chlorophyll differences were distributed southward along the western coast into CCB. In the spring, chlorophyll differences were the highest within the year in both magnitude (0.2 μg/l) and percentage (10%) (Figures 4.7-4.8).

In the summer and fall, nutrients were trapped below the thermocline with the effluent plume centering on the outfall (Figures 4.3-4.4). The dominant southwesterly winds produced offshore Ekman transport at the surface, onshore transport in the deep water, and upwelling at the coast. As a result, the effluent plume in bottom waters extended westward or northwestward toward BH and the North Shore area which could not be seen in the DIN distribution because of phytoplankton uptake. The time required for phytoplankton uptake and growth displaced the maximum chlorophyll difference 15-20 km away from the outfall, toward BH and the North Shore area. The additional chlorophyll entering the Harbor continued to take up nutrients and actually led to a slight decrease in Harbor DIN in July. Effluent contributed up to 5-10% of the bottom DIN in the summer, and up to about 10% chlorophyll with lower absolute differences than those of the spring. In the fall, both the magnitude and percentage of the chlorophyll differences were quite small.

Figure 4.6 shows nutrients and chlorophyll for the two simulations, averaged over the area of the control box shown in Figure 4.5. Figure 4.7 shows the difference between the simulations (Control minus NOS). Figure 4.8 shows that difference as a percent of the values in Figure 4.6. Addition of the outfall increased DIN and chlorophyll, as expected, but interestingly decreased silicate in the spring and summer. The reason for the negative influence on silicate is the low ratio of silicate to DIN in the outfall effluent (0.25). In the winter/spring period, the phytoplankton assemblage in the MBS was dominated by diatoms (e.g. Libby et al. 2006). Assuming diatoms contribute to 75% of the primary production and the Si/N uptake ratio is 1:1, every mole of DIN added would require 0.75 mole of silicate. Thus in the effluent plume, that phytoplankton assemblage had a 0.5

mole deficit of silicate that had to be supplied from the ambient waters. Therefore, addition of outfall silicate is insufficient to support the diatom growth that would be induced by the addition of outfall DIN.

4.2 A nutrient budget for May 2005

The massive red-tide (*Alexandrium spp*) blooms in May 2005 were also accompanied by strong phytoplankton blooms, especially after the second storm (Libby et al. 2006; Figures 3.3-3.5). Prior this bloom in the late spring, surface nutrient concentrations were low due to the spring bloom and vertical fluxes were low because of strong stratification. One interesting question is: What were the nutrient sources for phytoplankton blooms during this red-tide period?

The phytoplankton blooms in late spring 2005 (April-June) were associated with a series of extraordinary events in this region as evident from the model results, e.g., in the central Stellwagen Basin (Figure 4.9). In April, two strong river discharge events (not shown) brought large amount of fresh water into the MBS, which greatly reduced the salinity and enhanced the vertical stratification. Between May 7 and 9, the first Nor'easter pushed waters from the GOM into the MBS. The surface mixed layer deepened from 15–20 m prior to the storm to 40 m after the storm. The deepening of the mixed layer brought deep nutrient–rich waters into the surface mixed layer. The stratification was gradually restored and the mixed layer depth reduced to 20 m after the storm. Phytoplankton growth was enhanced. The nutrients in the surface mixed layer were depleted again before the second storm arrived on May 22. This second storm again brought in a large amount of GOM waters and deepened the mixed layer to 40 m. The deep flow from the GOM also supplied significant amount of nutrients (3rd panel, Figure 4.9), which were brought into the surface layer by vertical mixing or coastal upwelling. The stratification was restored in a few days after the storm probably due to the large freshwater discharge in the Merrimack River, as evident from the continuous decrease of both model and observed surface salinity at GoMOOS A after the storm (see Figure 3.17 in Jiang and Zhou 2008). A much stronger phytoplankton bloom followed this second storm. During this period, the only available measurements of primary productivity at N04 and N18 on May 13 gave an average value of 1.5 gC/m^2/day, which was similar to

the value during a spring bloom and much higher than the expected value this time of year. A primary production measurement on June 13 gave a mean value of 0.9 $gC/m^2/day$.

To further understand the cause for the phytoplankton blooms associated with these two storms, a simple DIN budget for the surface layer (upper 25m) was carried out. Though this is not an accurate mass balance, the sketch of mass balance based on limited data and some modeled results provided the first order estimates of nutrient sources. In this budget, a few assumptions or simplifications have been made: (1) nutrient concentrations in the rivers were derived from a multi-year average of available USGS data for the Merrimack River during this period; (2) the inputs of upstream rivers from New Hampshire and Maine coasts to the MBS were assumed equal to two times that of inputs from the Merrimack River simply due to a lack of data, and all nutrients from these were advected into MB; (3) nutrients from the MWRA outfall effluent were totally available for the upper water column as an upper limit, though in fact most of the effluent plume was trapped below the thermocline during this period (Figure 4.10); (4) the atmospheric loading was simply assumed to be half of the MWRA loading, though the former may be an under-estimate due to the heavy rains during the storm; (5) the vertical flux in the water column due to storm–induced mixing was simply calculated from the DIN concentrations in the surface layer (top 25m) before and after a storm and then divided by 15 days estimated from the beginning of the first storm to the beginning of the second storm; (6) because the nutrient gradients were small in the GOM offshore waters, the flux of GOM offshore waters would not change the DIN concentration; and (7) primary production throughout May 2005 was assumed to be 1.5 $gC/m^2/day$ and a Redfield C/N ratio of 6.625 was used to calculate the nitrogen uptake. The estimates of these fluxes and rates based on these assumptions are presented in Table 4.1.

The estimates indicate that the vertical mixing associated with these two storms contributed the majority (60%) of the nutrients for the primary production at the rate of 1.5 $gC/m^2/day$ in May 2005. Rivers and background vertical mixing supplied about 8% nutrients required by the primary production. The MWRA and atmospheric loadings contributed less than 2% each. The vertical mixing flux due to the deep mixing after the

first storm was able to contribute to the high production without nutrient limitation for 15 days.

Therefore, it can be further inferred that without the storms, the production in May 2005 would be less than 40% of the observed primary production, or about 0.6 $gC/m^2/day$. In this scenario, the DIN contribution from the effluent could be up to 5% if all nutrients were able to make it to the surface.

The spatial patterns of DIN and chlorophyll differences with and without effluent nutrients in May 2005 were similar to those in April: the DIN differences were mostly trapped below the thermocline and limited to within 15 km around the outfall; and the chlorophyll differences were concentrated along the western coast extending into CCB (Figure 4.10). The surface DIN increased associated with the two storms as indicated by the two spikes during May 2005 (Figure 4.8, top panel). In this period, the effluent contributed less than 3% to the surface DIN and about 7-8% to both surface and bottom chlorophyll. In a separate study of the 2005 *Alexandrium* bloom, Anderson et al. (2007) estimated that the effluent would increase at most 15% of the *Alexandrium* level in the downstream area, which was consistent with our estimate. Another dispersion model presented by Anderson et al. (2007) suggested a 10% *Alexandrium* increase by the effluent in a worst-case scenario, which was also consistent with our results.

Table 4.1. A simple budget of dissolved inorganic nitrogen in May 2005

Point Sources			
Local Rivers (Includes Merrimack, Charles, and Neponset Rivers)			
Nutrient Concentrations (μM)	40		USGS data
Flow (m_3/sec)		500	USGS data
flux (10^6 mol/day)		**1.8**	
Upstream Rivers (assumed to be twice the Local Rivers flux)			
flux (10^6 mol/day)		**3.6**	
MWRA effluent			
Flow (m3/sec)		20	MWRA data
Nutrient Concentrations (μM)	1000		MWRA data
flux (10^6 mol/day)		**1.7**	
Nonpoint Sources			
Atmospheric loading (assumed to be half MWRA daily loading)			
flux (10^6 mol/day)		**0.9**	
Vertical Mixing			
Background Mixing			
Mixing rate (cm^2/s)		0.1	Geyer & Ledwell (1997)
Vertical DIN differences (μM)	2		Model estimates
Vertical distance (m)		5	Model estimates
Surface Area (m^2)		$4.5x10^9$	Geyer et al. (1992)
flux (10^6 mol/day)		**1.6**	
Storms			
DIN (after-before) (μM)	1		Model estimates
Surface Volume (m^3)		$7.5*10^{11}$	Geyer et al. (1992)
Effective time (day)		15	The time between the two storms
flux (10^6 mol/day)		**50**	
Biological uptake			
Primary Production			
Primary productivity (gC/m^2/day)		1.5	MWRA data
Surface area (m^2)		$4.5x10^9$	Geyer et al. (1992)
C/N Redfield ratio (atoms C/N)	6.625		
flux (10^6 mol/day)		**85**	

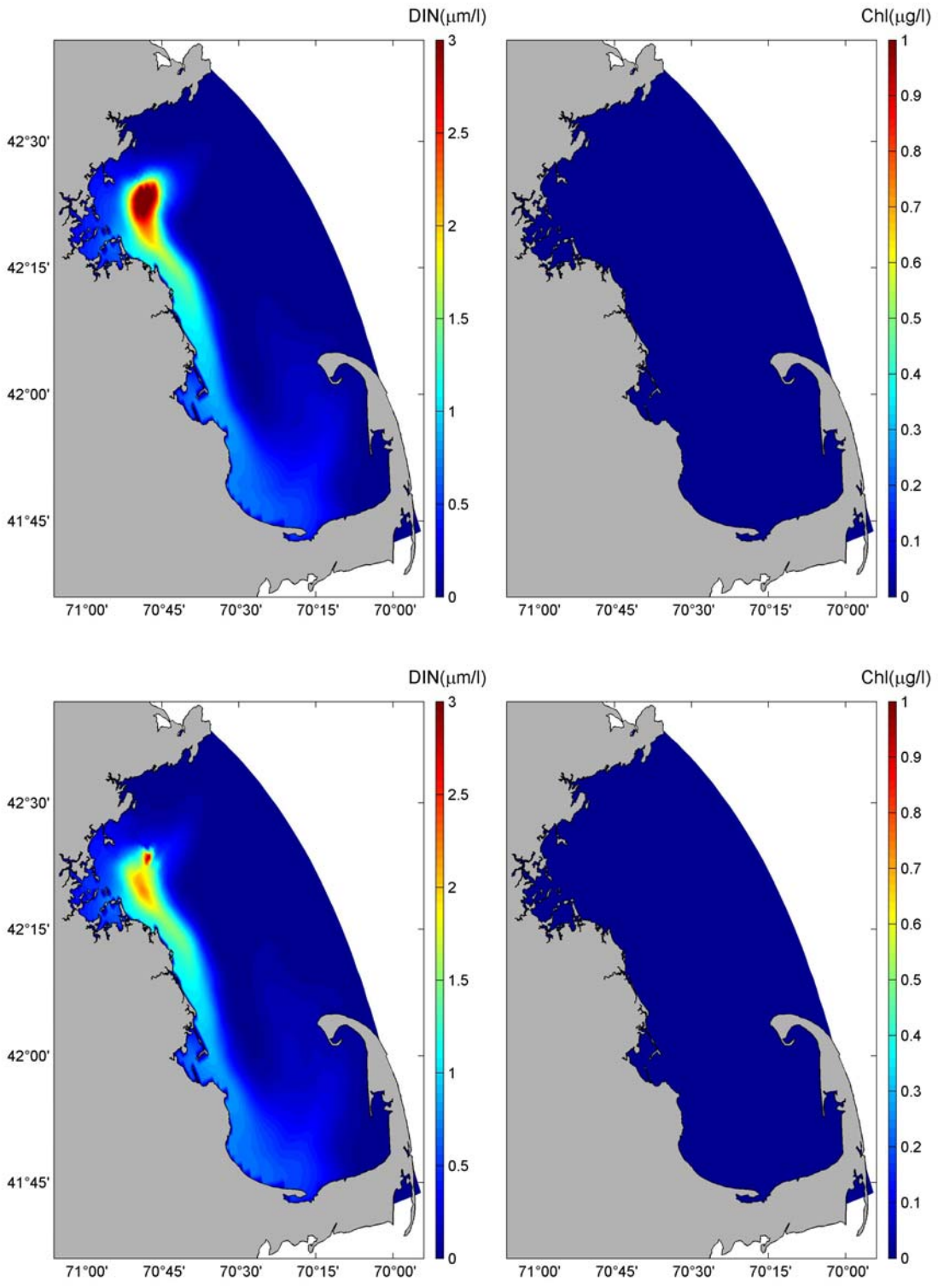

Figure 4.1 Monthly average difference of surface (top panels) and bottom (bottom panels) dissolved inorganic nitrogen (DIN) and chlorophyll (Chl) in January.

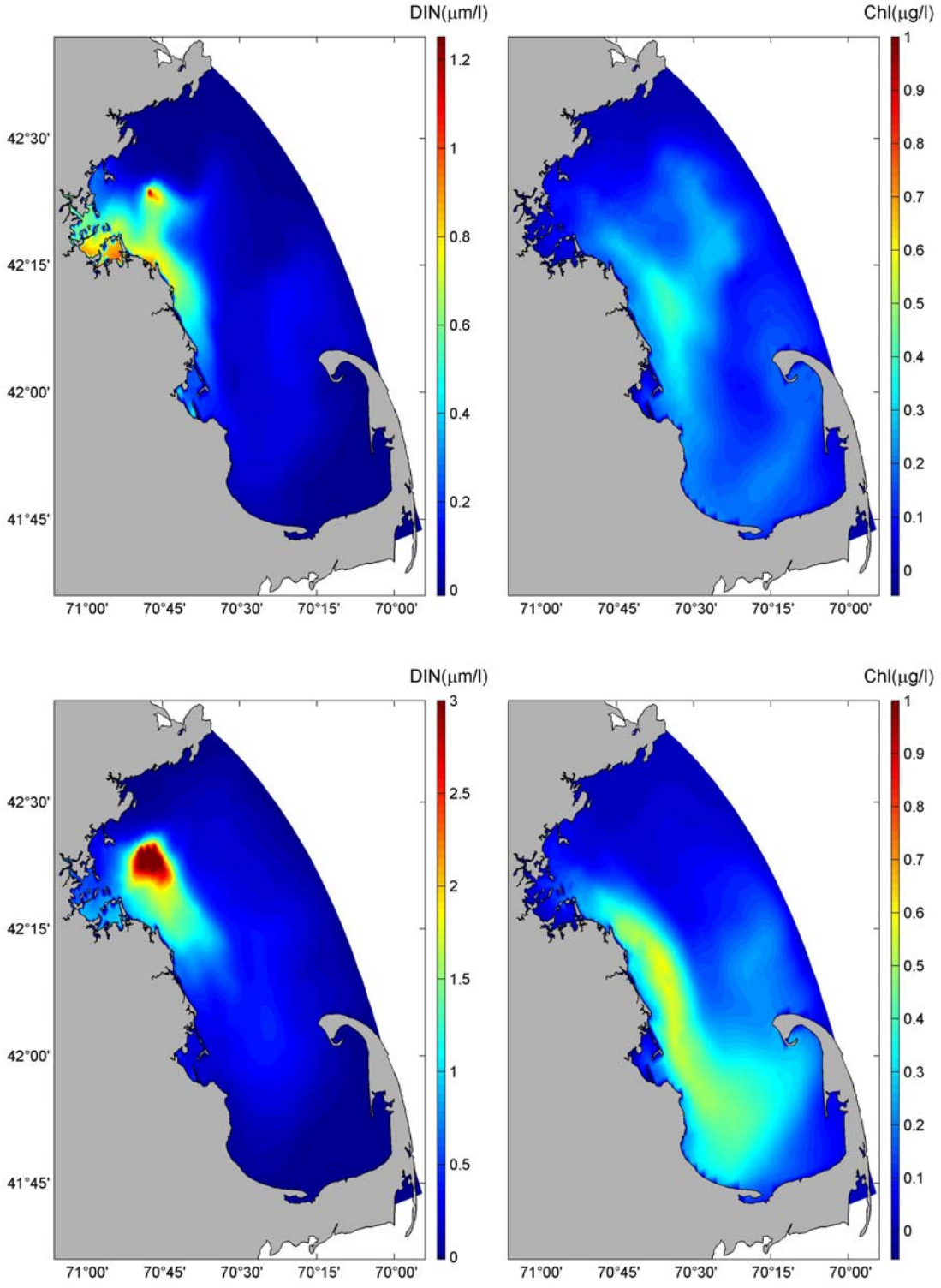

Figure 4.2. Monthly average difference of surface (top panels) and bottom (bottom panels) dissolved inorganic nitrogen (DIN) and chlorophyll (Chl) in April. Note the different color scales.

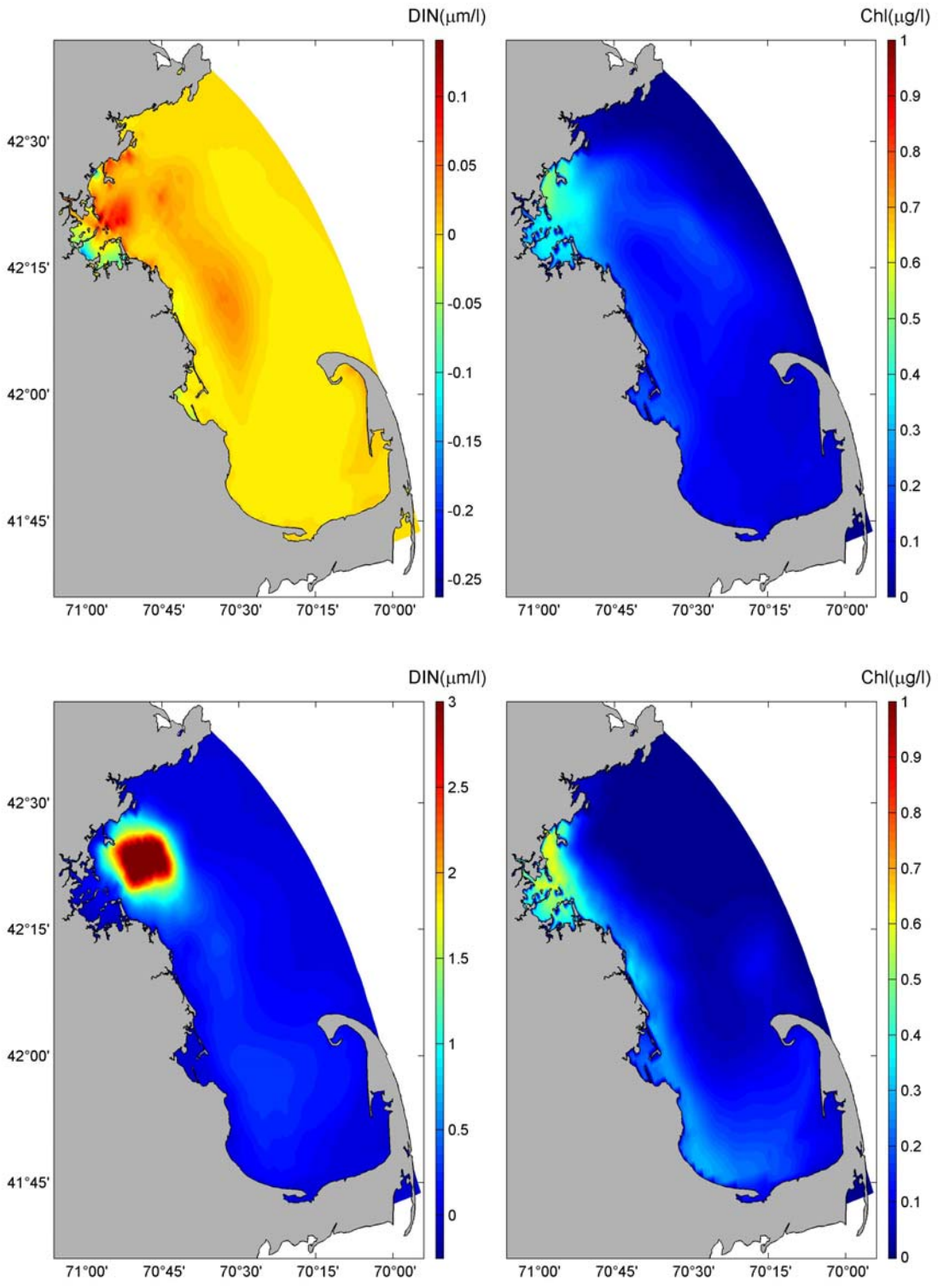

Figure 4.3. Monthly average difference of surface (top panels) and bottom (bottom panels) dissolved inorganic nitrogen (DIN) and chlorophyll (Chl) in July. Note the different color scales.

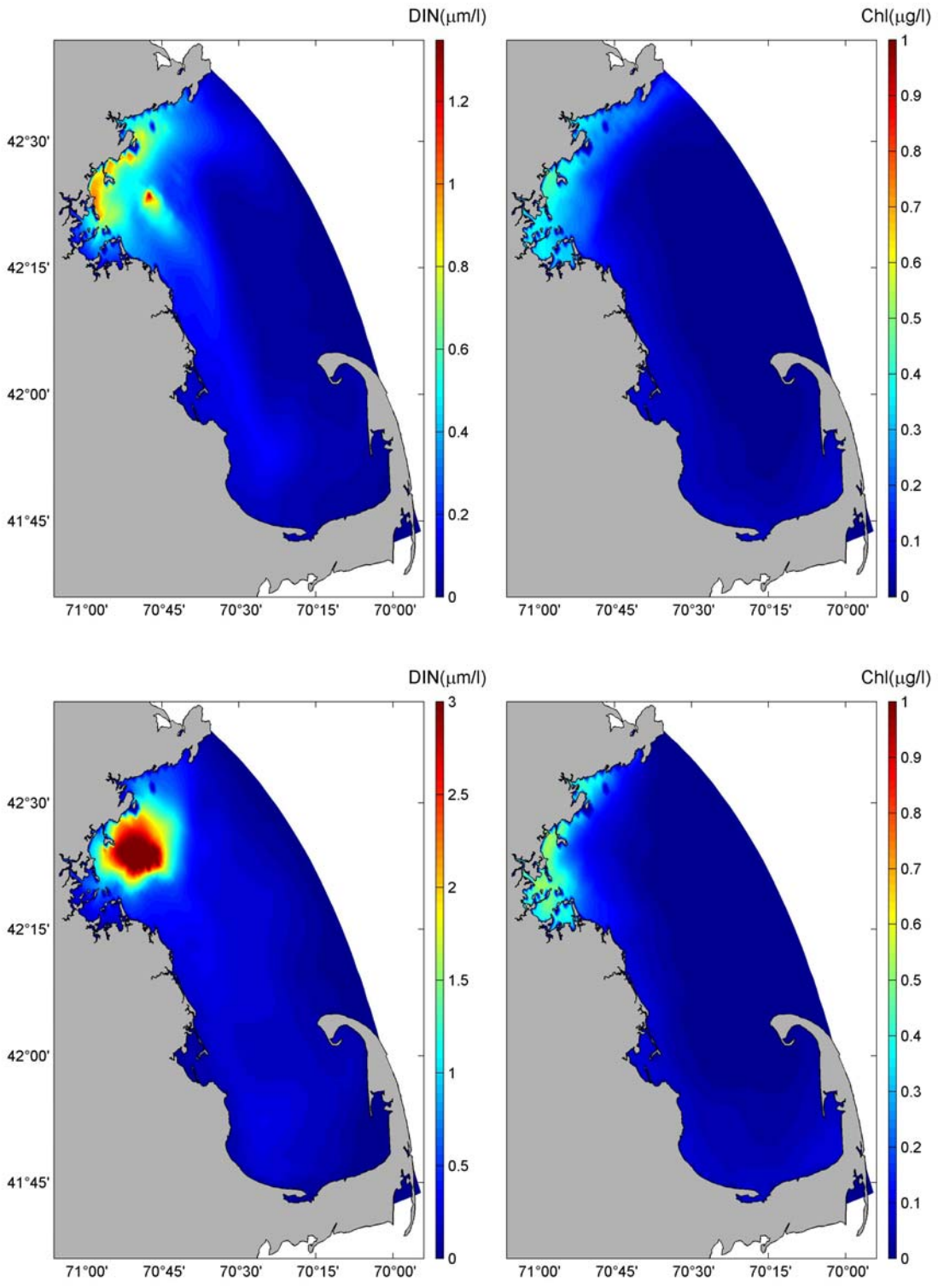

Figure 4.4. Monthly average difference of surface (top panels) and bottom (bottom panels) dissolved inorganic nitrogen (DIN) chlorophyll (Chl) in October. Note the different color scales.

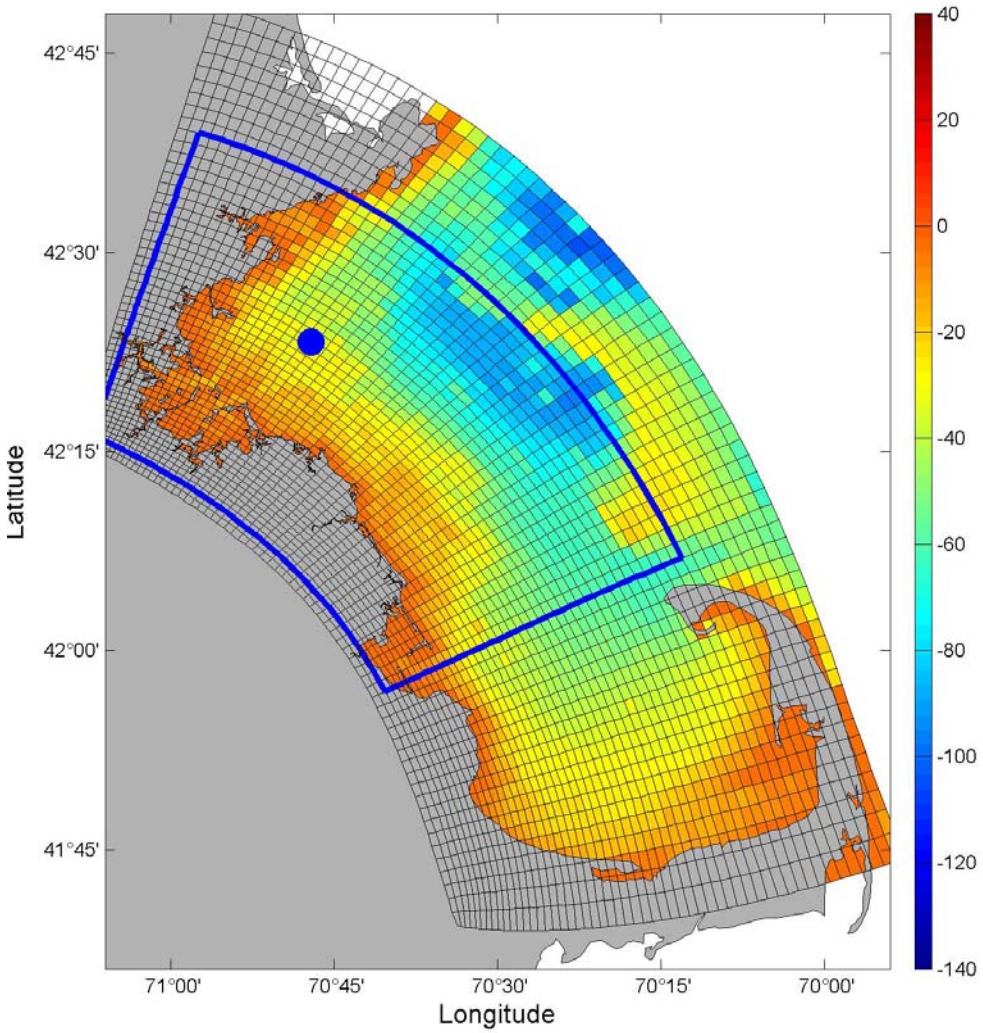

Figure 4.5. Box (blue solid line) used for average difference of chlorophyll and nutrients. Blue dot indicates the MWRA outfall.

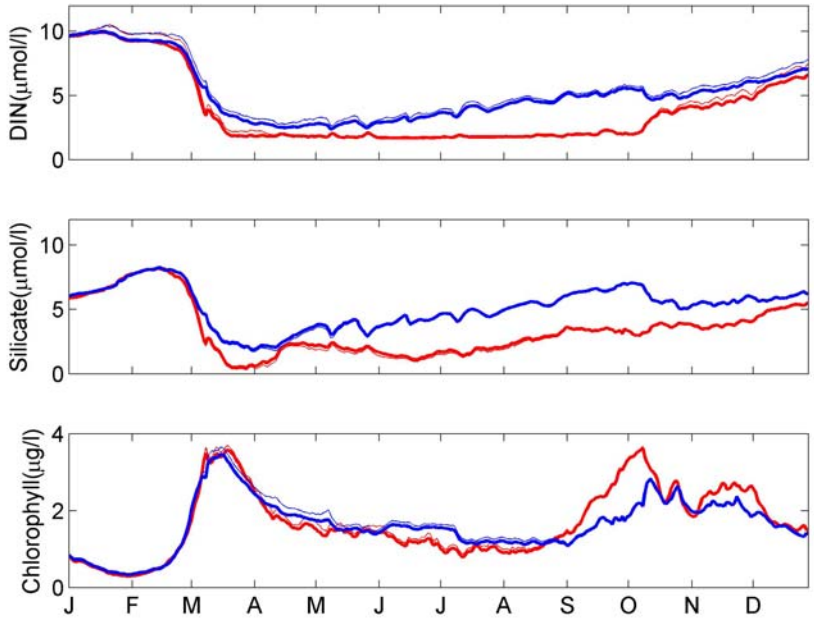

Figure 4.6. Box average surface and bottom DIN, silicate, and chlorophyll (Thin lines are the Control simulation (with the outfall); thick lines are the NOS simulation (without the outfall).).

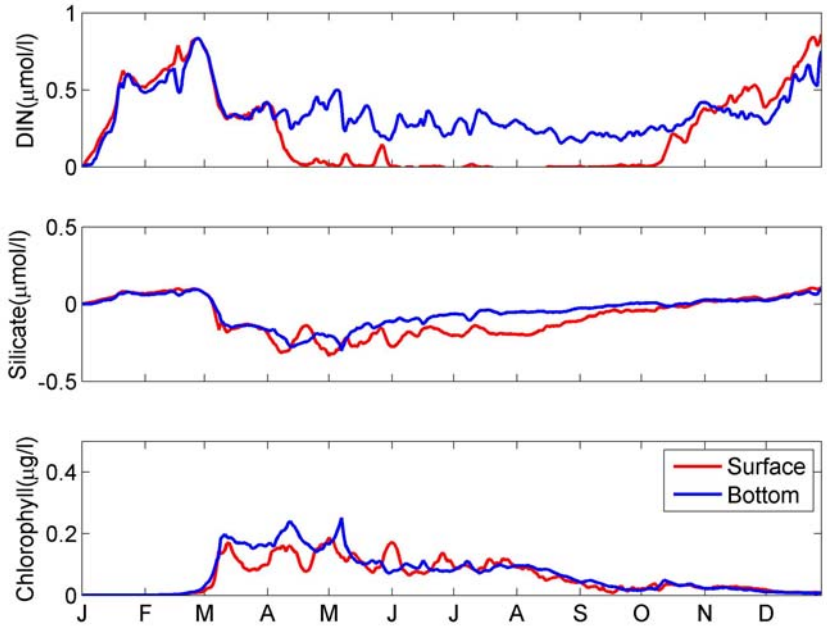

Figure 4.7. Box average difference of DIN, silicate, chlorophyll between the two model experiments (Control minus NOS).

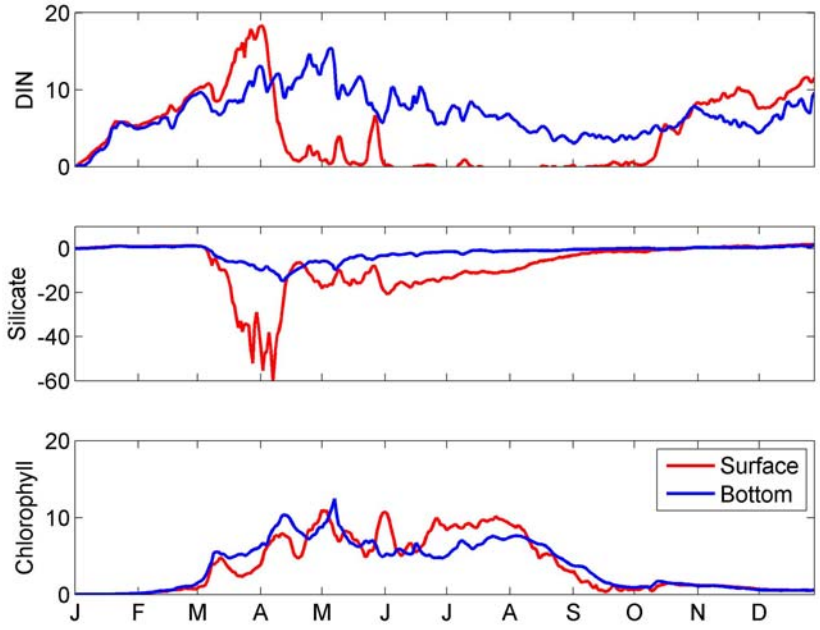

Figure 4.8. Percentages of average DIN, silicate, chlorophyll differences between the two model experiments relative to the means in control experiment ((Control minus NOS)/Control). In winter, effluent silicate contributes about +2%.

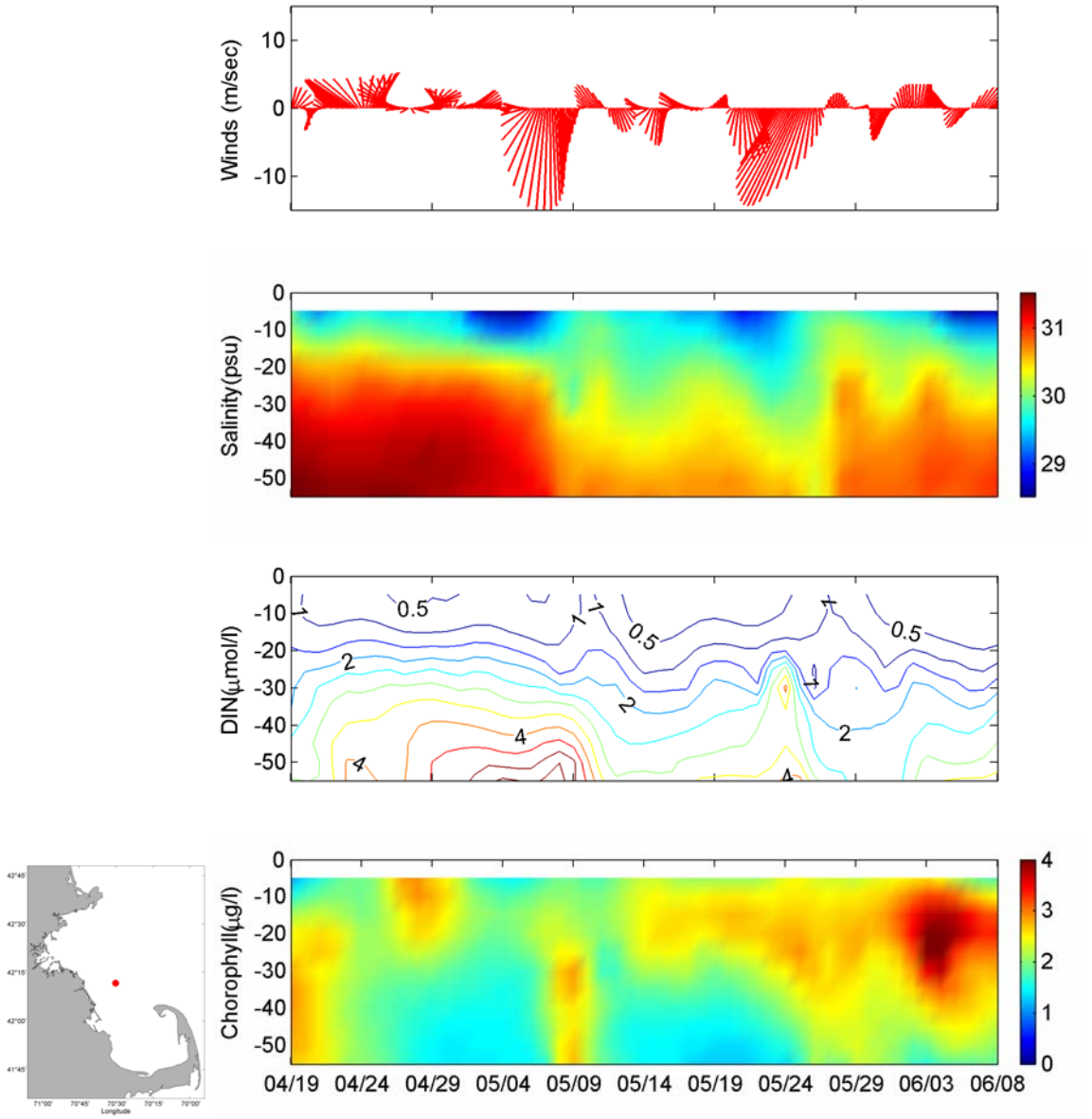

Figure 4.9 Time series of winds (NOAA 44013), salinity, chlorophyll, and DIN at a model grid point in the Stellwagen Basin. Left panel shows the location of the grid cell.

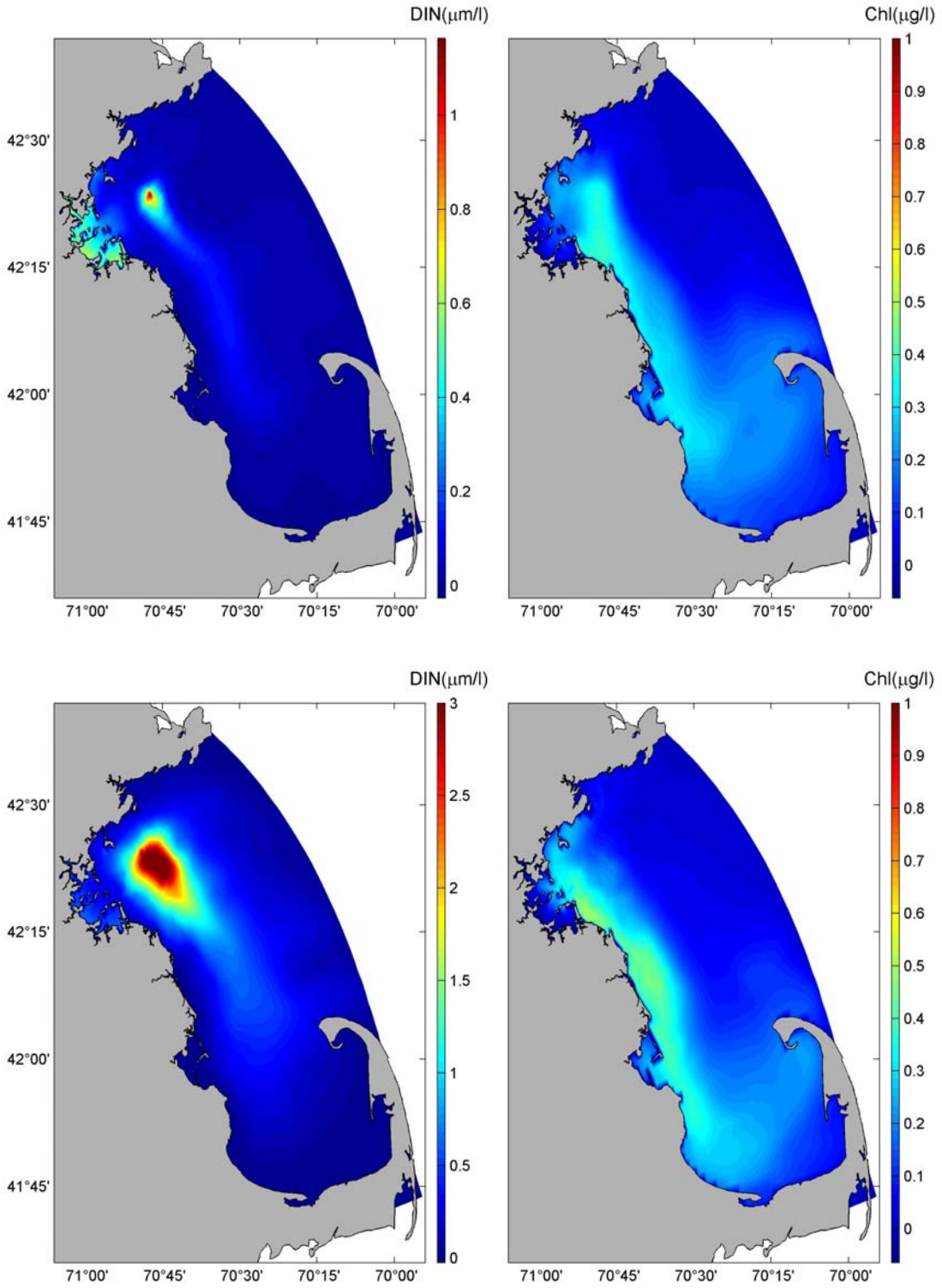

Figure 4.10. Monthly average difference of surface (top panels) and bottom (bottom panels) dissolved inorganic nitrogen (DIN) and chlorophyll (Chl) in May. Note the different color scales.

5. SUMMARY AND RECOMMENDATIONS

5.1 Summary

This study compared the modeled water quality variables from the 2005 BEM simulation with observed ones. The results also described seasonal and short–term physical, biological and chemical environment and processes in the water column and sediments in the MBS in response to seasonal forcing and two Nor'easter storms in May 2005. With more forcing data collected during the 2005 red-tide event, the modeled physical and biogeochemical variables (except chlorophyll) compared better with observed than in some past years as suggested from the 1:1 correlations between modeled and observed key variables.

The model has difficulty in simulating chlorophyll and bottom PON concentrations in general, and primary production in summer. The causes for these mismatches between model and observed results are complicated by the natural complexity of an ecosystem, uncertainties in empirical formulation, and limitations of model schemes and resolution.

Our analysis suggests that there was a strong seasonal cycle in the spatial patterns and concentrations attributable to MWRA effluent nutrients in 2005. In the spring, the GOM current intrusion and northerly/northeasterly winds supported a southward coastal current transporting the effluent plume southward along the western coast of Massachusetts Bay. During the summer and fall, the effluent plume was usually trapped below the thermocline, but at times when the prevailing winds were out of the southwest, effluent derived nutrients along with ambient bottom water nutrients were upwelled along the western and northwestern coastlines of the bay. The effluent may lead to increases in local DIN and chlorophyll concentrations less than 20% and 10%, respectively, during spring, and less than 10% in the remainder of the year.

A nutrient budget analysis for May 2005 suggests that the vertical mixing in two Nor'easter wind storms contributed the great majority of nutrient loading into the surface mixed layer. The estimates indicate that the vertical mixing associated with these two storms contributed the majority (60%) of the new nutrients supporting primary production at the high rate of 1.5 gC/m2/day observed. Rivers and background vertical

mixing supplied about 8% of the nutrients required by the primary production. The MWRA and atmospheric loading contributed less than 2% each. The vertical mixing flux due to the deep mixing after the first storm was able to contribute to a high production without nutrient limitation for 15 days.

5.2 Recommendations

Based on this and previous simulations, we recommend 3 future studies:

1. Mesoscale physical-biogeochemical processes. Mesoscale processes such as eddies, filaments and coastal jets frequently take place in the MBS due to complex interactions between winds, the GOM intruding currents, freshwater plumes and topography. These processes are difficult to resolve by regular monthly surveys with a survey distance of 10-20 km between 2 stations. Studies on these mesoscale physical-biogeochemical processes will not only improve the predictive capability of the BEM, but also strengthen the entire monitoring program.

2. Retrospective studies. With more than 10 years of monitoring and numerical modeling, retrospective studies can bring insight into the mechanisms leading the occurrences of specific events such as the *Phaeocystis* bloom in 2004, the missing blooms in spring 1998 and fall 2004, and the large red-tide event in late spring 2005. For example, the analysis of nutrient budgets during the 2005 red-tide event helps us understand the late spring phytoplankton bloom, which has important implications to zooplankton and higher trophic level ecological processes. With better understanding of these events, the models can then be improved and better predict their occurrence.

3. Improving the boundary conditions. We continue to recommend enhancement of monitoring efforts for biogeochemical processes near the open boundary. Heavy reliance on empirical assumptions is unavoidable during model assimilation of a few scattered observations. We recommend increasing horizontal and vertical coverage for biogeochemical parameters along the boundary for effectively improving model open boundary conditions.

6. REFERENCES

Adams, E. E., J. W. Hansen, R. L. Lago, P. Clayton, and X. Zhang (1992), A simple box model of the nitrogen cycle in Boston Harbor and the Massachusetts Bays, *Civil Engr. Pract.*, *fall 1992*, 91-103.

Anderson DM, Libby PS, Mickelson MJ, Borkman DG and McGillicuddy DJ. 2007. The 2005 New England red tide of Alexandrium fundyense: observations, causes, and potential outfall linkages. Boston: Massachusetts Water Resources Authority. Report 2007-10. 85 p.

Becker, S. (1992), The seasonal distribution of nutrients in Massachusetts and Cape Cod Bays, MS thesis, University of New Hampshire, 127pp.

Bienfang, P.K., P.J. Harrison and L. M. Quarmby (1982), Sinking rate response to depletion of nitrate, phosphate and silicate in four marine diatoms, *Marine Biology*, *67*, 295-302.

Bigelow, H.B. 1927, Physical oceanography of the Gulf of Maine (Part II). Bulletin of the Bureau of Fisheries, 40: 511-1027.

Butman, B., Bothner, M.H. Lightsom, F.L. Gutierrez, B.T., Alexander, P.S., Martini, M.A., and Strahle, W.S., 2002, Long-term Oceanographic Observations in Western Massachusetts Bay offshore of Boston, Massachusetts: Data Report for 1989-2000, U.S. Geological Survey Digital Data Series 74.

Culver, M.E., and W.O. Smith, Jr. (1989), Effects of environmental variables on sinking rates of marine phytoplankton, *J. Phycol*., *25*, 262-270.

Di Toro, D. M. 2001, *Sediment Flux Modeling*, Wiley-Interscience, New York, 624 pp.

Geyer, W. R., Gardner, G. B., Brown, W. S., Irish, J., Butman, B., Loder, T., and Signell, R. P. 1992, Physical oceanographic investigation of Massachusetts and Cape Cod Bays. Massachusetts Bay Program. MBP-92-03, 497pp.

Geyer W. R. and Ledwell J. R. 1997. Boundary mixing in Massachusetts Bay. Boston: Massachusetts Water Resources Authority. Report 1997-09. 20 p.

Hendry, R., and I. He (1996), *Technical report on objective analysis (OA) project*, Bedford Institute of Oceanography, Dartmouth, Nova Scotia, 105pp.

HydroQual, Inc. 2000, Bays Eutrophication Model (BEM): modeling analysis for the period 1992-1994. Boston, Massachusetts Water Resources Authority. ENQUAD 2000-02, 158pp.

HydroQual, Inc. 2003, Bays Eutrophication Model (BEM): modeling analysis for the period 1998-1999. Boston, Massachusetts Water Resources Authority. ENQUAD 2003-03, 318pp.

HydroQual, Inc. and Normandeau Associates, Inc. 1995, A water quality model for Massachusetts and Cape Cod Bays: Calibration of the Bay Eutrophication Model (BEM). Boston, Massachusetts WAter Resource Authority. ENQUAD 1995-08, 402pp.

HydroQual, Inc. and Signell, R.P. 2001, Calibration of the Massachusetts and Cape Cod Bays Hydrodynamic Model: 1998-1999. Boston, Massachusetts Water Resources Authority. ENQUAD 2001-12, 170pp.

Hyer, P.V., C. S. Fang, E. P. Ruzeck, and W. J. Hargis (1971), Hydrography and hydrodynamics of Virginia estuaries, studies of the distribution of salinity and dissolved oxygen in the upper York system, Virginia Institute of Marine Science.

Jiang, M.S. and Zhou, M. 2004a. Calibration of the Massachusetts and Cape Cod Bays hydrodynamic model: 2000-2001. Boston, Massachusetts Water Resources Authority. Draft Report. ENQUAD 2004-08. 71pp.

Jiang, M.S. and M. Zhou, 2004b, Bays Eutrophication Model: 2000-2001 simulation. Boston: Massachusetts Water Resources Authority. Report 2004-09. 71 p.

Jiang, M.S. and M. Zhou, 2006a, Massachusetts Bay hydrodynamic model: 2002-2004 simulation. Boston: Massachusetts Water Resources Authority. Report 2006-12. 128 p.

Jiang, M.S. and M. Zhou, 2006b, Massachusetts Bays Eutrophication Model: 2002-2004 simulation. Boston: Massachusetts Water Resources Authority. Report 2006-13. 126p.

Jiang, M.S. and M. Zhou, 2008, Massachusetts Bay hydrodynamic model: 2005 simulation. Boston: Massachusetts Water Resources Authority. Report 2008-12. 57p.

Kropp, R. K., Diaz, R., Dahlen, D., Boyle, J. D., and Hunt, C. D. 2002, 2001 Harbor Benthic Monitoring Report. Boston, Massachusetts Water Resources Authority. ENQUAD 2002-19, 74pp.

Kropp, R. K., Diaz, R., Hecker, B., Dahlen, D., Boyle, J. D., Abramson, S. L., and Emsbo-Mattingly, S. 2001, 2000 Outfall Benthic Monitoring Report. Boston, Massachusetts Water Resources Authority. ENQUAD 2001-14, 148pp.

Laws, E. A., and M. S. Chalup (1990), A microalgal growth model, *Limnol. Oceanogr.*, *35*, 597-608.

Libby, P. S., Hunt, C. D, Geyer, W. R., Keller, A. A., Oviatt, C. A., and Turner, J. T. 2000, 1999 Annual Water Column Monitoring Report. Boston, Massachusetts Water Resources Authority. ENQUAD 2000-09, 180pp.

Libby, P. S., Hunt, C. D, McLeod, L. A., Geyer, W. R., Keller, A. A., Borkman, D., Oviatt, C. A., and Turner, J. T. 2001, 2000 Annual Water Column Monitoring Report. Boston, Massachusetts Water Resources Authority. ENQUAD 2001-17, 196pp.

Libby, P.S., Geyer W.R., Keller A.A., Turner J.T., Borkman D., Mickelson M.J., Hunt C.D., Oviatt C.A. 2002**.** 2001 Annual Water Column Monitoring Report. Boston: Massachusetts Water Resources Authority. Report ENQUAD 2002-22. 100pp.

Libby PS, Geyer WR, Keller AA, Mansfield AD, Turner JT, Anderson DM, Borkman D, Rust SW, Hyde, K, Oviatt CA. 2006**.** 2005 Annual Water Column Monitoring Report. Boston: Massachusetts Water Resources Authority. Report ENQUAD 2006-20. 182 p

Lynch, D.R., Naimie, C.E. and Werner, F.E., 1996. Comprehensive coastal circulation model with appliction to the Gulf of Maine. Cont. Shelf Res., 12: 37-64.

Maciolek, N. J., Diaz, R. J., Dahlen, D., Hecker, B., Gallagher, E. D., Blake, J. A., Williams, I. P., Emsbo-Mattingly, S., Hunt, C., and Keay, K. E. 2003, 2002 Outfall Benthic Monitoring Report. Boston, Massachusetts Water Resources Authority. ENQUAD 2003-13, 166pp.

Menzie-Cura & Associates, 1991, Sources and Loadings of Pollutants to Massachusetts Bay. Prepared for the Massachusetts Bay Program, Massachusetts Coastal Zone Management, US. EPA. Technical Report NO. MBP-91-01.

Signell, R.P., Jenter, H.L., and Blumberg, A.F., 1996. Circulation and effluent dilution modeling in Massachusetts Bay: model implementation, verification and results. USGS Open File Report 96-015, U.S. Geological Survey, Woods Hole.

Signell, R. P., H. L. Jenter, and A. F. Blumberg. 2000, Predicting the physical effects of relocating Boston's sewage outfall, *J. Estuar. Coast. Shelf Sci*., *50*, 59-72.

Smolarkiewicz, P. K., 1984, A fully multidimensional positive definite advection transport algorithm with implicit diffusion. *J. Comput. Phys.*, **54**, 325-362.

Taylor D.I. 2004. Harbor-Bay eutrophication-related water chemistry changes after 'offshore transfer'. Boston: Massachusetts Water Resources Authority. Report 2004-06. 83 p.

Tucker J, S. Kelsey, A.E. Giblin, and C.S. Hopkinson, 2006, 2005 annual benthic nutrient flux monitoring report. Boston: Massachusetts Water Resources Authority. Report 2006-17. 69 p.

Turner, J.T., 1994, Planktonic Copepods of Boston Harbor, Massachusetts Bay and Cape-Cod Bay, 1992. *Hydrobiologia*. 293: 405-413.

Appendix A. Model kinetic equations for nitrogen

Here we outline the biogeochemical processes simulated in the BEM. Notations and descriptions of model parameters are listed in Table 2.2 and will not be described below.

1) Phytoplankton (P_c) growth is determined by net growth (μ), sinking loss (k_{sp}) and grazing loss (k_{grz}),

$$G_p = \left(\mu - k_{sp}(T) - k_{grz}(T)\right)P_C \tag{A1}$$

where T denotes the ambient water temperature.

The specific net growth rate μ of phytoplankton is defined as,

$$\mu = \left(\mu_{\max} G_T(T) - k_{RB}\right)G_N(N) \tag{A2}$$

where $\mu_{\max}$ is nutrient-saturated growth rate, $G_T(T)$ is temperature correction factor, and $G_N(N)$ is nutrient limitation factor.

Temperature dependence of phytoplankton growth is determined by,

$$G_T(T) = \begin{cases} \exp\left(-\beta_1\left(T - T_{OPT}\right)^2\right) & T \le T_{OPT} \\ \exp\left(-\beta_2\left(T_{OPT} - T\right)^2\right) & T \ge T_{OPT} \end{cases} \tag{A3}$$

Nutrient uptake follows Liebig's law with the limitation of individual nutrient determined by Michaelis-Menten kinetics,

$$G_N(N) = \min\left(\frac{DIN}{k_N + DIN}, \frac{DIP}{k_P + DIP}, \frac{Si}{k_{Si} + Si}\right) \tag{A4}$$

where *DIN* is total dissolved inorganic nitrogen, *DIP* is total dissolved inorganic phosphorus and Si is dissolved silicic acid (silicate).

Nutrient saturated growth rate ($\mu_{\max}$) is based on the balance growth model developed by Laws and Chalup (1990),

$$\mu_{\max} = \frac{G_{pre}(1-k_{RG})(1-f_{SC})I)}{G_{pre}/G_{pr0} + I(1+G_{pre}/(I_S G_{pr0}))} \tag{A5}$$

where $I(z,t)$ is solar radiation.

Chlorophyll to carbon ratio is also following the formulation by Laws and Chalup (1990),

$$a_{ChlC} = \frac{1-(1-QF)(1-\mu/\mu_{\max}) - f_{SC} - (\mu + k_{RB})(1-k_{RG})G_{pre}}{W_{CChl}} \tag{A6}$$

and phytoplankton endogenous respiration is determined by,

$$k_{PR} = \frac{k_{RB} + k_{RG}\mu}{1-k_{RG}} \tag{A7}$$

The total primary productivity is determined by,

$$GPP = (\mu + k_{PR})P_c \tag{A8}$$

and total respiration and grazing is,

$$Loss = (k_{PR} + k_{grz}(T))P_c \tag{A9}$$

2) Light

Light attenuation accounts for background attenuation and phytoplankton self-shading,

$$k_{ext} = k_{base} + k_c a_{ChlC} P_{tot} \tag{A10}$$

where P_{tot} is total phytoplankton biomass of the three phytoplankton groups. Thus the solar radiation at depth z (upward positive with origin at sea surface) is,

$$I(z,t) = I_{surf}(t)\exp\left(\int_0^z k_{ext}\,dz\right) \tag{A11}$$

where $I_{surf}(t)$ is surface solar radiation that can be calculated from daily mean solar radiation (I_{tot}),

$$I_{surf}(t) = \frac{I_{tot}}{0.635 f} \sin\left(\frac{\pi(t - t_{sunrise})}{f}\right) \quad \text{(A12)}$$

The saturation solar radiation is determined by the average light level for the previous three days,

$$I_s = \left(I_{tot_{n-3}} + I_{tot_{n-2}} + I_{tot_{n-1}}\right)/3 \quad \text{(A13)}$$

3) Algal settling (Bienfang et al., 1982; Culver and Smith, 1989),

$$k_{sp}(T) = \left(V_b + V_N\left(1 - G_N(N)\right)\right)\theta_{sp}^{(T-20)} / H \quad \text{(A14)}$$

4) Zooplankton grazing

$$k_{grz}(T) = k_{grz0}\theta_{grz}^{(T-20)} \quad \text{(A15)}$$

5) Hydrolysis of particulate organic matter to dissolved organic nitrogen

$$R_{LPON} = k_{LPON}\theta_{LPON}^{T-20} \frac{P_{tot}}{K_{mp} + P_{tot}} LPON \quad \text{(A16a)}$$

$$R_{RPON} = k_{RPON}\theta_{RPON}^{T-20} \frac{P_{tot}}{K_{mp} + P_{tot}} RPON \quad \text{(A16b)}$$

6) Mineralization of dissolved organic nitrogen to ammonia

$$R_{LDON} = k_{LDON}\theta_{LDON}^{T-20} \frac{P_{tot}}{K_{mp} + P_{tot}} LDON \quad \text{(A17a)}$$

$$R_{RDON} = k_{RDON}\theta_{RDON}^{T-20} \frac{P_{tot}}{K_{mp} + P_{tot}} RDON \quad \text{(A17b)}$$

7) Nitrification

$$R_{Nit} = k_{Nit}\theta_{Nit}^{T-20} \frac{DO}{k_{Nit\_DO} + DO} NH_3 \quad \text{(A18)}$$

8) Denitrification

$$R_{Denit} = k_{Denit}\theta_{Denit}^{T-20}\frac{k_{Denit\_DO}}{k_{Denit\_DO}+DO}NO_3 \quad \text{(A19)}$$

9) Exudation of total primary productivity (*GPP*) into dissolved organic carbon

$$R_{exud} = a_{NC} f_{ExDOC} GPP \quad \text{(A20)}$$

10) Nitrogen to carbon ratio

$$a_{NC} = \frac{QF + (1-QF)\,\mu/\mu_{\max}}{W_{CN}} \quad \text{(A21)}$$

11) Settling of particulate organic nitrogen

$$k_{PON}(T) = \frac{V_{PON}}{H}\theta_{PON}^{T-20} \quad \text{(A22)}$$

Massachusetts Water Resources Authority
Charlestown Navy Yard
100 First Avenue
Boston, MA 02129
(617) 242-6000
http://www.mwra.state.ma.us